
VaSST: VARIATIONAL INFERENCE FOR SYMBOLIC REGRESSION USING SOFT SYMBOLIC TREES

Somjit Roy*

Department of Statistics
Texas A&M University
College Station, TX 77843
sroy_123@tamu.edu

Pritam Dey

Department of Statistics
Texas A&M University
College Station, TX 77843
pritam.dey@tamu.edu

Bani K. Mallick

Department of Statistics
Texas A&M University
College Station, TX 77843
bmallick@stat.tamu.edu

ABSTRACT

Symbolic regression has recently gained traction in AI-driven scientific discovery, aiming to recover explicit closed-form expressions from data that reveal underlying physical laws. Despite recent advances, existing methods remain dominated by heuristic search algorithms or data-intensive approaches that assume low-noise regimes and lack principled uncertainty quantification. Fully probabilistic formulations are scarce, and existing Markov chain Monte Carlo-based Bayesian methods often struggle to efficiently explore the highly multimodal combinatorial space of symbolic expressions. We introduce VaSST, a scalable probabilistic framework for symbolic regression based on *variational inference*. VaSST employs a continuous relaxation of symbolic expression trees, termed *soft symbolic trees*, where discrete operator and feature assignments are replaced by soft distributions over allowable components. This relaxation transforms the combinatorial search over an astronomically large symbolic space into an efficient gradient-based optimization problem while preserving a coherent probabilistic interpretation. The learned soft representations induce posterior distributions over symbolic structures, enabling principled uncertainty quantification. Across simulated experiments and Feynman Symbolic Regression Database within SRBench, VaSST achieves superior performance in both structural recovery and predictive accuracy compared to state-of-the-art symbolic regression methods.

Keywords Symbolic Regression; Scientific Machine Learning; Uncertainty Quantification; Black-box Variational Inference; Automatic Differentiation.

1 Introduction

Symbolic regression for scientific discovery. *Scientific Machine Learning* (SciML) has emerged as a powerful paradigm for integrating domain knowledge with data-driven modeling, enabling advances across materials science [Butler et al., 2018], climate and weather prediction [Zhang et al., 2025], biology [Boadu et al., 2025], and physics [Raissi et al., 2019]. A central objective in these domains is the discovery of explicit governing equations that encode mechanistic structure rather than merely predictive relationships. In this setting, *symbolic regression* (SR) plays a pivotal role. Unlike classical prediction-centric regression methods [Tibshirani, 1996, Rasmussen and Williams, 2006, Chipman et al., 2010], SR operates directly over functional forms to recover concise, structurally interpretable mathematical expressions from experimental data. By identifying explicit equations underlying complex scientific phenomena, SR has enabled sparse discovery of nonlinear dynamical systems [Brunton et al., 2016], accelerated materials design [Wang et al., 2024], and uncovered fundamental scientific laws [Schmidt and Lipson, 2009].

Related work. Existing SR methods can be broadly categorized into *evolutionary*, *machine learning*-based, and *Bayesian* approaches. Classical SR is dominated by *genetic programming* and related heuristic search algorithms [Davidson et al., 2003, Fortin et al., 2012, Stephens, 2016], which explore expressions through stochastic evolution but often

*Corresponding author.

suffer from high computational complexity, sensitivity to initialization, and the generation of overly complex formulas [Korns, 2011]. More recent machine learning-driven methods cast SR as a sequential decision-making problem, learning to generate grammar rules, tree traversals, or executable symbolic strings via neural architectures [Udrescu and Tegmark, 2020, Petersen et al., 2021, Broløf et al., 2021, Kamienny et al., 2022]. Although these methods enhance scalability and predictive performance, they remain inherently search-driven and computationally challenging due to the NP-hard nature of symbolic space exploration [Virgolin and Pissis, 2022]. Moreover, their effectiveness is often contingent on large training datasets and low-noise regimes, as we demonstrate in Section 5. This review highlights that fully probabilistic formulations of SR remain limited.

Note that, scientific expressions possess an inherently hierarchical and compositional structure that aligns naturally with tree representations (see Figure 1). Tree models are ubiquitous in modern machine learning for capturing nonlinear interactions with strong predictive performance [Breiman et al., 1984, Breiman, 1996], while Bayesian tree formulations [Chipman et al., 1998, Densin et al., 1998, Chipman et al., 2010] provide a coherent inferential framework through priors over structures, principled model comparison, and uncertainty quantification. In context of SR, the *Bayesian Machine Scientist* (BMS) [Guimerà et al., 2020] represents an important step toward Bayesian equation discovery. However, it employs an ad hoc structural prior built from corpus parsing based on a priori knowledge, and performs inference using *Metropolis-Hastings* (MH) proposals over discrete symbolic tree structures. Given the highly multimodal and combinatorial posterior landscape, such local MH updates can exhibit poor mixing in complex discrete spaces [Bhamidi et al., 2008, Łatuszyński et al., 2025], leading to slow convergence and inefficient exploration of the symbolic model space. Similarly, *Bayesian Symbolic Regression* (BSR) [Jin et al., 2020] adopts a tree-based partial Bayesian formulation but uses plug-in ordinary least squares estimates for regression parameters. This incomplete parameter uncertainty propagation, combined with local stochastic MH structural updates, further impedes effective traversal of the symbolic model space and frequently produces overly complicated output expressions, as evidenced in Section 5.

Our contributions. In light of these drawbacks, we propose a *variational inference* framework for SR that combines principled Bayesian modeling with improved computational scalability over existing probabilistic SR methods. Variational inference recasts Bayesian inference as an optimization problem [Blei et al., 2017], offering a scalable alternative to traditional Monte Carlo-based approaches for modern data-intensive settings [Jordan et al., 1999, Blei et al., 2003, Wainwright and Jordan, 2008, Graves, 2011]. However, a naïve application of variational inference over the discrete structural space of symbolic expressions results in a combinatorial optimization problem that negates these scalability benefits [Williams, 1992, Koza, 1994].

To overcome this challenge, we introduce a novel representation of symbolic expressions using *soft symbolic trees*, in which each operator and feature assignment is replaced by a soft combination over all allowable operators and features. This relaxation transforms the discrete structural search into a continuous optimization problem, enabling efficient gradient-based exploration of the symbolic model space through *black-box* variational inference [Ranganath et al., 2014, Kucukelbir et al., 2017, Giordano et al., 2024]. Structural interpretability is preserved by mapping the learned soft representations to *hard* symbolic trees through a *randomized* post-optimization procedure. This continuous relaxation trick is similar in spirit to soft relaxations used for variational inference in decision tree-based regression [Salazar, 2023]. However, in context of SR the soft representations naturally induce probability distributions over hard symbolic tree structures, thereby providing a principled mechanism for quantifying uncertainty in the recovered symbolic expressions. We refer to this framework as, VaSST: *Variational Inference for Symbolic Regression using Soft Symbolic Trees*.

A primary goal in scientific equation discovery is to favor structural parsimony in accordance to the *Occam’s razor* principle [Jefferys and Berger, 1992]. VaSST achieves this by controlling structural complexity via a *depth-dependent regularizing prior* that penalizes overly complex symbolic expressions. Through extensive experiments, we demonstrate that VaSST effectively balances structural discovery and predictive accuracy while maintaining computational stability, outperforming a range of state-of-the-art symbolic regression methods. A Python implementation of VaSST is available at anonymous.4open.science/r/VaSST-62C7.

2 Symbolic Tree Representation of Scientific Expressions

Scientific expressions can be constructed by combining primary features (e.g., x_1, x_2) and mathematical operators (e.g., $\exp, \sin, +, \times$). We denote the full set of p primary features as \mathcal{X} and the set of allowed mathematical operators as $\mathcal{O} = \mathcal{O}_u \cup \mathcal{O}_b$, where \mathcal{O}_u and \mathcal{O}_b contain the unary and binary operators, respectively. Typical choices in scientific modeling include, $\mathcal{O}_u = \{\sin, \cos, \exp, ^2, ^3\}$ and $\mathcal{O}_b = \{+, \times, -, /\}$ [Udrescu and Tegmark, 2020].

Let \mathcal{E} denote the set of admissible feature-operator compositions. Any symbolic expression $\mathfrak{E} \in \mathcal{E}$ is defined recursively as one of, (a) *primitive expression*: $\mathfrak{E} = x_1$, where $x_1 \in \mathcal{X}$; (b) *binary composition*: $\mathfrak{E} = b(\mathfrak{E}_1, \mathfrak{E}_2)$, where $\mathfrak{E}_1, \mathfrak{E}_2 \in \mathcal{E}$

and $b \in \mathcal{O}_b$, for e.g., $x_1 + x_2$; and (c) *unary composition*: $\mathfrak{E} = u(\tilde{\mathfrak{E}})$, where $\tilde{\mathfrak{E}} \in \mathcal{E}$ and $u \in \mathcal{O}_u$, for e.g., $\exp(x_1)$. This set of characterizations naturally maps each $\mathfrak{E} \in \mathcal{E}$ to a symbolic tree structure $\mathcal{T}(\mathfrak{E})$, where *internal (nonterminal)* nodes either represent unary (with 1 child node) or binary (with 2 children nodes) operators, while *leaves (terminal nodes)* correspond to primary features from \mathcal{X} ; see Figure 1. It is important to note that, unlike decision tree-based models [Breiman et al., 1984, Chipman et al., 2010], which recursively partition the input feature space, our framework interprets symbolic trees as compositional structures that assign input features from \mathcal{X} to leaves and operators from \mathcal{O} to internal nodes. Such tree representations of symbolic expressions are not necessarily unique, for e.g., $x_1(x_2 + x_3)$ is treated to be same as that of $x_1x_2 + x_1x_3$, in our framework.

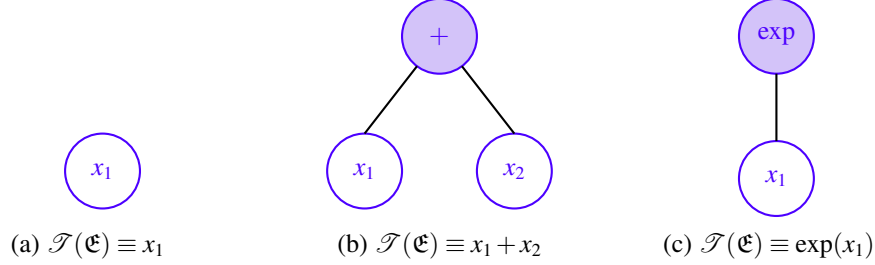


Figure 1: Symbolic tree representation.

Now, for $\mathfrak{E} \in \mathcal{E}$ and an instance $\mathbf{x} \in \mathbb{R}^p$ of the features in \mathcal{X} , we define $g(\mathbf{x}; \mathcal{T}(\mathfrak{E}))$ to be the real-valued evaluation of the symbolic expression $\mathcal{T}(\mathfrak{E})$ at \mathbf{x} . With this setup in place, we formally present the VaSST modeling framework.

3 The VaSST Model

We outline the VaSST model which comprises two major components: (i) a *symbolic ensemble* consisting of a linear regression of the response variable over a forest of K symbolic trees and (ii) a hierarchical prior specification over the model regression coefficients, the model noise variance, and the symbolic tree structures.

3.1 The Symbolic Ensemble Component

Let $\mathcal{D}_n := \{(\mathbf{x}_i, y_i)\}_{i=1}^n$ be the collection of observed data units. VaSST models and structurally learns the hidden symbolic relationship between the responses $y_i \in \mathbb{R}$ and primary features in $\mathbf{x}_i \in \mathbb{R}^p$ by using a collection of K symbolic trees, $\{\mathcal{T}(\mathfrak{E}_j)\}_{j=1}^K$, evaluated at \mathbf{x}_i , as:

$$y_i = \beta_0 + \sum_{j=1}^K g_j(\mathbf{x}_i) \beta_j + \varepsilon_i, \quad i = 1, \dots, n, \quad (1)$$

where $g_j(\mathbf{x}_i) = g(\mathbf{x}_i; \mathcal{T}(\mathfrak{E}_j))$, $\boldsymbol{\beta} = (\beta_0, \dots, \beta_K)^\top \in \mathbb{R}^{K+1}$ is the model regression coefficient vector, and $\varepsilon_i \in \mathbb{R}$ is the model noise with $\varepsilon_i \sim \mathcal{N}_1(0, \sigma^2)$ independently. From (1), we obtain the vector representation of the symbolic ensemble component:

$$\mathbf{y} = \mathbf{T}\boldsymbol{\beta} + \boldsymbol{\varepsilon}, \quad \boldsymbol{\varepsilon} \sim \mathcal{N}_n(0_n, \sigma^2 \mathbf{I}_n), \quad (2)$$

where $\mathbf{T} = (g_j(\mathbf{x}_i))_{1 \leq i \leq n, 0 \leq j \leq K} \in \mathbb{R}^{n \times \overline{K+1}}$ is the *expression design matrix*, $g_0(\mathbf{x}_i) = 1$ for all $i = 1, \dots, n$, $\mathbf{y} = (y_1, \dots, y_n)^\top \in \mathbb{R}^n$ is the response vector, and $\boldsymbol{\varepsilon} = (\varepsilon_1, \dots, \varepsilon_n)^\top \in \mathbb{R}^n$ is the model noise vector.

The model regression parameters $(\boldsymbol{\beta}, \sigma^2)$ jointly are endowed upon with the conjugate Normal Inverse-Gamma (NIG) prior viz., $\boldsymbol{\beta} \mid \sigma^2 \sim \mathcal{N}_{K+1}(\boldsymbol{\mu}_0, \sigma^2 \boldsymbol{\Sigma}_0)$ and $\sigma^2 \sim \text{IG}(a_0, b_0)$, where $\boldsymbol{\mu}_0 \in \mathbb{R}^{K+1}$, $\boldsymbol{\Sigma}_0$ (positive definite matrix of order $K+1$), and $a_0, b_0 > 0$ are the hyperparameters of the Normal and Inverse-Gamma prior distributions, respectively. We complete the VaSST model specification by describing the symbolic tree prior in Section 3.2.

3.2 The VaSST Symbolic Tree Prior

The VaSST symbolic tree probability model for each $\mathcal{T}(\mathfrak{E}_j)$ is constructed in two stages: (a) a probabilistic specification over a *maximal binary tree skeleton* and (b) a *deterministic pruning operation* that maps the skeleton tree to a valid symbolic tree, as depicted in Figure 2.

Full binary tree skeleton. To decouple structural decisions from operator and feature assignments, we embed each symbolic tree $\mathcal{T}(\mathfrak{E}_j)$ into a full binary tree skeleton, denoted by $\mathcal{S}_j^{(D)}$, of fixed maximum depth $D \in \mathbb{N}$. Let $\mathcal{Z}_D = \{0, 1, \dots, N-1\}$ index the skeleton tree nodes in *heap order*, where 0 is the root and the left and right children of a skeleton node $\zeta \in \mathcal{Z}_D$ are given by $L(\zeta) = 2\zeta + 1$ and $R(\zeta) = 2\zeta + 2$, respectively. The total number of nodes is $N = 2^{D+1} - 1$. Also, let $d_\zeta \in \{0, \dots, D\}$ denote the depth of node ζ . For each skeleton node $\zeta \in \mathcal{Z}_D$, we introduce the following, (a) *expansion indicator*: $e_{j\zeta} \in \{0, 1\}$, where $e_{j\zeta} = 1$ or $e_{j\zeta} = 0$ indicates that ζ is an internal node or a leaf of $\mathcal{T}(\mathfrak{E}_j)$, respectively; (b) *operator assignment*: $o_{j\zeta} \in \mathcal{O}$, specifies the operator assigned to ζ if $e_{j\zeta} = 1$; and (c) *feature assignment*: $h_{j\zeta} \in \mathcal{X}$, specifies the primary feature assigned to ζ if $e_{j\zeta} = 0$.

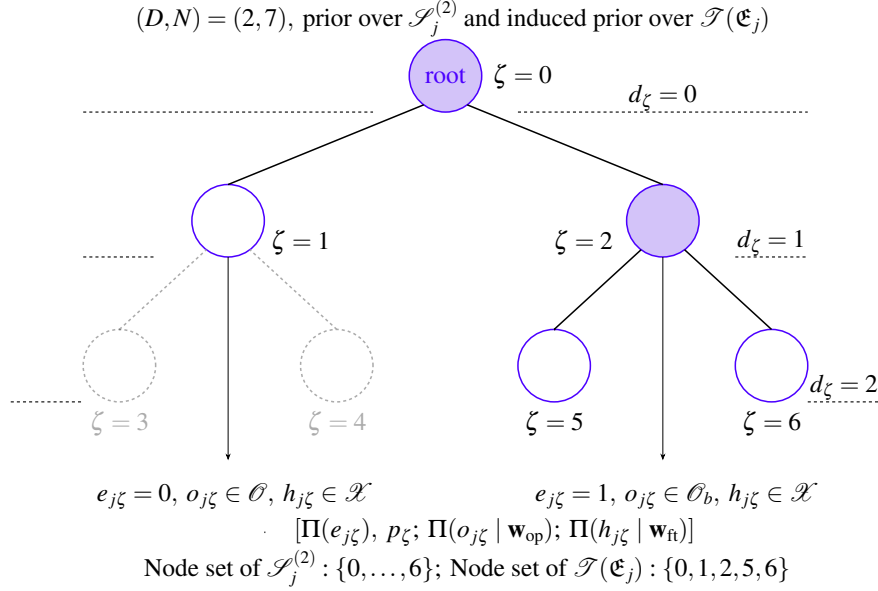


Figure 2: A live representation of the prior over $\mathcal{S}_j^{(2)}$ and the induced prior over $\mathcal{T}(\mathfrak{E}_j)$. In $\mathcal{S}_j^{(2)}$, the children nodes $\zeta = 3, 4$ of $\zeta = 1$ are pruned using \mathfrak{p} as $e_{j1} = 0$ to obtain the valid symbolic tree $\mathcal{T}(\mathfrak{E}_j)$.

Valid symbolic tree via deterministic pruning. The skeleton $\mathcal{S}_j^{(D)}$ is an *ambient* representation. We obtain the corresponding valid symbolic tree $\mathcal{T}(\mathfrak{E}_j)$ by applying a deterministic pruning operator \mathfrak{p} which proceeds as follows, (a) *terminal pruning*: if $e_{j\zeta} = 0$, then all descendants of ζ in the skeleton are removed, making it a leaf; and (b) *unary operator pruning*: if $e_{j\zeta} = 1$ and $o_{j\zeta} \in \mathcal{O}_u$, then the right subtree rooted at $R(\zeta)$ is removed. Thus, the resulting symbolic tree is $\mathcal{T}(\mathfrak{E}_j) = \mathfrak{p}(\mathcal{S}_j^{(D)})$.

Prior over full binary tree skeleton. The prior specification over $\mathcal{S}_j^{(D)}$ is characterized by the prior over the latent skeleton variables, $\{e_{j\zeta}, o_{j\zeta}, h_{j\zeta} : \zeta \in \mathcal{Z}_D\}$, as follows:

$$\begin{aligned}
 e_{j\zeta} &\sim \text{Ber}(p_\zeta), \quad p_\zeta = \alpha(1 + d_\zeta)^{-\delta}, \\
 o_{j\zeta} | \mathbf{w}_{\text{op}} &\sim \text{Cat}(\mathbf{w}_{\text{op}}), \quad \mathbf{w}_{\text{op}} \sim \text{Dir}(\boldsymbol{\eta}_{\text{op}}), \\
 h_{j\zeta} | \mathbf{w}_{\text{ft}} &\sim \text{Cat}(\mathbf{w}_{\text{ft}}), \quad \mathbf{w}_{\text{ft}} \sim \text{Dir}(\boldsymbol{\eta}_{\text{ft}}),
 \end{aligned} \tag{3}$$

where $j = 1, \dots, K$, $\alpha \in (0, 1)$, $\delta > 0$, and $\text{Ber}(\cdot)$, $\text{Cat}(\cdot)$, and $\text{Dir}(\cdot)$ represents the Bernoulli, Categorical, and Dirichlet distributions, respectively. In (3), $\mathbf{w}_{\text{op}} \in \Delta^{|\mathcal{O}|}$ and $\mathbf{w}_{\text{ft}} \in \Delta^p$ are the operator and feature weight vectors, where $\Delta^m = \{\mathbf{z} \in [0, \infty)^m \mid \mathbf{1}_m^\top \mathbf{z} = 1\}$ is the m -dimensional simplex; and $\boldsymbol{\eta}_{\text{op}} \in (0, \infty)^{|\mathcal{O}|}$ and $\boldsymbol{\eta}_{\text{ft}} \in (0, \infty)^p$ are the Dirichlet concentration hyperparameters. Therefore, using (3) the prior specification over $\Theta = (\{\mathcal{S}_j^{(D)}\}_{j=1}^K, \mathbf{w}_{\text{op}}, \mathbf{w}_{\text{ft}})$ is:

$$\Pi(\Theta) = \Pi(\mathbf{w}_{\text{op}})\Pi(\mathbf{w}_{\text{ft}}) \prod_{j=1}^K \prod_{\zeta \in \mathcal{Z}_D} \Pi(e_{j\zeta})\Pi(o_{j\zeta} | \mathbf{w}_{\text{op}})\Pi(h_{j\zeta} | \mathbf{w}_{\text{ft}}). \tag{4}$$

Note that, the prior over the skeleton $\mathcal{S}_j^{(D)}$ in (4) induces a prior over $\mathcal{T}(\mathfrak{E}_j)$. We conclude with Remark 1 emphasizing the importance of the *depth-dependent split probability* in (3) as a mechanism for controlling symbolic expression complexity.

Remark 1 (Depth-dependent split probability). *Guided by the Occam’s razor principle [Jefferys and Berger, 1992], we aim to learn interpretable and parsimonious symbolic expressions which adequately captures the underlying scientific mechanism. This is achieved by the depth-dependent split probability p_ζ in (3) which imparts a regularizing effect on the individual tree depths [Chipman et al., 1998].*

4 Variational Inference for VaSST

Combining the data likelihood $p(\mathbf{y} | \mathbf{T}, \boldsymbol{\beta}, \sigma^2)$, the joint prior over the model regression parameters in Section 3.1, and the VaSST symbolic tree prior in Section 3.2, the joint posterior distribution induced over all unknowns $(\Theta, \boldsymbol{\beta}, \sigma^2)$ is:

$$\Pi(\Theta, \boldsymbol{\beta}, \sigma^2 | \mathcal{D}_n) \propto p(\mathbf{y} | \mathbf{T}, \boldsymbol{\beta}, \sigma^2) \Pi(\boldsymbol{\beta}, \sigma^2) \Pi(\mathbf{w}_{\text{op}}) \Pi(\mathbf{w}_{\text{ft}}) \prod_{j=1}^K \prod_{\zeta \in \mathcal{Z}_D} \Pi(e_{j\zeta}) \Pi(o_{j\zeta} | \mathbf{w}_{\text{op}}) \Pi(h_{j\zeta} | \mathbf{w}_{\text{ft}}). \quad (5)$$

Marginalization over model regression parameters. The conjugate NIG prior over $(\boldsymbol{\beta}, \sigma^2)$ enables marginalization in (5) and results into: $\Pi(\Theta | \mathcal{D}_n) \propto p(\mathbf{y} | \mathbf{T}) \Pi(\Theta)$, where $p(\mathbf{y} | \mathbf{T})$ up to constants is:

$$\log p(\mathbf{y} | \mathbf{T}) = \frac{1}{2} \log |\boldsymbol{\Sigma}_n| - a_n \log b_n + \log \Gamma(a_n), \quad (6)$$

where $\Gamma(\cdot)$ is the Gamma function, $|\boldsymbol{\Sigma}_n|$ is the determinant of the matrix $\boldsymbol{\Sigma}_n$, and:

$$\begin{aligned} \boldsymbol{\Sigma}_n^{-1} &= \boldsymbol{\Sigma}_0^{-1} + \mathbf{T}^\top \mathbf{T}, \quad \boldsymbol{\mu}_n = \boldsymbol{\Sigma}_n (\boldsymbol{\Sigma}_0^{-1} \boldsymbol{\mu}_0 + \mathbf{T}^\top \mathbf{y}), \quad a_n = a_0 + \frac{n}{2}, \\ b_n &= b_0 + \frac{1}{2} (\mathbf{y}^\top \mathbf{y} + \boldsymbol{\mu}_0^\top \boldsymbol{\Sigma}_0^{-1} \boldsymbol{\mu}_0 - \boldsymbol{\mu}_n^\top \boldsymbol{\Sigma}_n^{-1} \boldsymbol{\mu}_n). \end{aligned} \quad (7)$$

See Appendix G.1 for complete derivations. Therefore, it remains to draw inference from $\Pi(\Theta | \mathcal{D}_n)$.

Variational family. To conduct scalable and efficient inference, we adopt a variational inference routine for approximating the posterior $\Pi(\Theta | \mathcal{D}_n)$ with a tractable *variational family* $q_\phi(\Theta)$ in (8) below, parameterized by variational parameters in ϕ [Blei et al., 2017]. Specifically, we choose a *mean-field* factorization [Jordan et al., 1999]:

$$\begin{aligned} q_\phi(\Theta) &= q_\phi(\mathbf{w}_{\text{op}}) q_\phi(\mathbf{w}_{\text{ft}}) \prod_{j=1}^K \prod_{\zeta \in \mathcal{Z}_D} q_\phi(e_{j\zeta}) q_\phi(o_{j\zeta}) q_\phi(h_{j\zeta}), \\ q_\phi(e_{j\zeta}) &\equiv \text{Ber}(e_{j\zeta}; \tilde{p}_{j\zeta}), \\ q_\phi(o_{j\zeta}) &\equiv \text{Cat}(o_{j\zeta}; \tilde{\pi}_{j\zeta}^{\text{op}}), \quad q_\phi(h_{j\zeta}) \equiv \text{Cat}(h_{j\zeta}; \tilde{\pi}_{j\zeta}^{\text{ft}}), \\ q_\phi(\mathbf{w}_{\text{op}}) &\equiv \text{Dir}(\tilde{\boldsymbol{\eta}}_{\text{op}}), \quad q_\phi(\mathbf{w}_{\text{ft}}) \equiv \text{Dir}(\tilde{\boldsymbol{\eta}}_{\text{ft}}), \end{aligned} \quad (8)$$

for $j = 1, \dots, K$ and $\zeta \in \mathcal{Z}_D$, where:

$$\begin{aligned} \text{logit}(\tilde{p}_{j\zeta}) &= \log \frac{\tilde{p}_{j\zeta}}{1 - \tilde{p}_{j\zeta}} = \ell_{j\zeta}, \quad \ell_{j\zeta} \in \mathbb{R} \\ \tilde{\pi}_{j\zeta}^{\text{op}} &= \text{softmax}(\mathbf{a}_{j\zeta}^{\text{op}}), \quad \text{softmax}(\mathbf{a}_{j\zeta}^{\text{op}})_o = \frac{\exp(a_{j\zeta,o}^{\text{op}})}{\sum_{o=1}^{|\mathcal{O}|} \exp(a_{j\zeta,o}^{\text{op}})}, \quad o = 1, \dots, |\mathcal{O}|, \quad \mathbf{a}_{j\zeta}^{\text{op}} \in \mathbb{R}^{|\mathcal{O}|}, \\ \tilde{\pi}_{j\zeta}^{\text{ft}} &= \text{softmax}(\mathbf{a}_{j\zeta}^{\text{ft}}), \quad \text{softmax}(\mathbf{a}_{j\zeta}^{\text{ft}})_k = \frac{\exp(a_{j\zeta,k}^{\text{ft}})}{\sum_{k=1}^p \exp(a_{j\zeta,k}^{\text{ft}})}, \quad k = 1, \dots, p, \quad \mathbf{a}_{j\zeta}^{\text{ft}} \in \mathbb{R}^p. \end{aligned}$$

Hence, ϕ collects the parameters $\tilde{\boldsymbol{\eta}}_{\text{op}}, \tilde{\boldsymbol{\eta}}_{\text{ft}}, \ell_{j\zeta}, \mathbf{a}_{j\zeta}^{\text{op}}$, and $\mathbf{a}_{j\zeta}^{\text{ft}}$.

Evidence lower bound. The variational parameters in ϕ are obtained by maximizing the *evidence lower bound* (ELBO):

$$\mathcal{L}(\phi) = \mathbb{E}_{q_\phi}[\log p(\mathbf{y} | \mathbf{T})] - \text{KL}(q_\phi(\Theta) \| \Pi(\Theta)), \quad (9)$$

where the Kullback-Leibler (KL) divergence is: $\text{KL}(q_\phi(\Theta) \parallel \Pi(\Theta)) = \int q_\phi(\Theta) \log(q_\phi(\Theta)/\Pi(\Theta)) d\Theta$. Now, we focus on the KL term in (9). Note that, owing to the mean-field variational family in (8), $\text{KL}(q_\phi(\Theta) \parallel \Pi(\Theta))$ splits as:

$$\begin{aligned} \text{KL}(q_\phi(\Theta) \parallel \Pi(\Theta)) &= \text{KL}(q_\phi(\mathbf{w}_{\text{op}}) \parallel \Pi(\mathbf{w}_{\text{op}})) + \text{KL}(q_\phi(\mathbf{w}_{\text{ft}}) \parallel \Pi(\mathbf{w}_{\text{ft}})) \\ &+ \sum_{j=1}^K \sum_{\zeta \in \mathcal{Z}_D} \left[\text{KL}(q_\phi(e_{j\zeta}) \parallel \Pi(e_{j\zeta})) + \mathbb{E}_{q_\phi(\mathbf{w}_{\text{op}})} [\text{KL}(q_\phi(o_{j\zeta}) \parallel \Pi(o_{j\zeta} \mid \mathbf{w}_{\text{op}}))] \right. \\ &\left. + \mathbb{E}_{q_\phi(\mathbf{w}_{\text{ft}})} [\text{KL}(q_\phi(h_{j\zeta}) \parallel \Pi(h_{j\zeta} \mid \mathbf{w}_{\text{ft}}))] \right], \end{aligned} \quad (10)$$

where:

$$\begin{aligned} \text{KL}(q_\phi(e_{j\zeta}) \parallel \Pi(e_{j\zeta})) &= \bar{p}_{j\zeta} \log \frac{\bar{p}_{j\zeta}}{p_\zeta} + (1 - \bar{p}_{j\zeta}) \log \frac{1 - \bar{p}_{j\zeta}}{1 - p_\zeta}, \\ \text{KL}(q_\phi(\mathbf{w}_{\text{op}}) \parallel \Pi(\mathbf{w}_{\text{op}})) &= \log(\mathcal{B}(\boldsymbol{\eta}_{\text{op}})/\mathcal{B}(\tilde{\boldsymbol{\eta}}_{\text{op}})) + \sum_{k=1}^{|\mathcal{O}|} (\tilde{\eta}_{\text{op},k} - \eta_{\text{op},k}) (\Psi(\tilde{\eta}_{\text{op},k}) - \Psi(\mathbf{1}_{|\mathcal{O}|}^\top \tilde{\boldsymbol{\eta}}_{\text{op}})), \\ \mathbb{E}_{q_\phi(\mathbf{w}_{\text{op}})} [\text{KL}(q_\phi(o_{j\zeta}) \parallel \Pi(o_{j\zeta} \mid \mathbf{w}_{\text{op}}))] &= \sum_{k=1}^{|\mathcal{O}|} \tilde{\pi}_{j\zeta,k}^{\text{op}} \left[\log(\tilde{\pi}_{j\zeta,k}^{\text{op}}) - \Psi(\tilde{\eta}_{\text{op},k}) + \Psi(\mathbf{1}_{|\mathcal{O}|}^\top \tilde{\boldsymbol{\eta}}_{\text{op}}) \right], \end{aligned} \quad (11)$$

where $\mathcal{B}(\cdot)$ and $\Psi(\cdot)$ are the multivariate Beta and Digamma functions, respectively. Also, $\text{KL}(q_\phi(\mathbf{w}_{\text{ft}}) \parallel \Pi(\mathbf{w}_{\text{ft}}))$ and $\mathbb{E}_{q_\phi(\mathbf{w}_{\text{ft}})} [\text{KL}(q_\phi(h_{j\zeta}) \parallel \Pi(h_{j\zeta} \mid \mathbf{w}_{\text{ft}}))]$ are given analogously to the last two expressions in (4); see Appendix G.2 for details.

The term $\mathbb{E}_{q_\phi}[\log p(\mathbf{y} \mid \mathbf{T})]$ in (9) does not admit an analytical form. A direct stochastic optimization is computationally prohibitive due to the combinatorial nature of the structural variables $\{e_{j\zeta}, o_{j\zeta}, h_{j\zeta} : \zeta \in \mathcal{Z}_D\}_{j=1}^K$. The induced discrete model space grows exponentially with both tree depth (D) and ensemble size (K) having $O((2p^{|\mathcal{O}|})^{N \cdot K})$ possible configurations. Combinatorial search over this astronomically large space is therefore infeasible. Moreover, gradient-based optimization over discrete variables would require high-variance score-function estimators [Williams, 1992, Ranganath et al., 2014] or specialized structured search procedures [Koza, 1994, Schmidt and Lipson, 2009], both of which scale poorly and become impractical even for moderate values of D and K . To overcome this computational bottleneck, VaSST introduces a differentiable relaxation of symbolic trees, regarded as *soft symbolic trees*, transforming discrete structural and labeling decisions into continuous approximations [Maddison et al., 2017, Liu et al., 2019].

Soft symbolic trees via continuous relaxations. To construct soft symbolic trees, i.e., $\mathcal{S}_j^{(D)} \rightarrow \mathcal{S}_j^{\text{soft}}$ for $j = 1, \dots, K$, we implement the *Binary Concrete* [Maddison et al., 2017] and *Gumbel-Softmax* [Jang et al., 2016] *continuous relaxations* on the discrete structural variables $\{e_{j\zeta}, o_{j\zeta}, h_{j\zeta} : \zeta \in \mathcal{Z}_D\}_{j=1}^K$ as follows:

$$\begin{aligned} \text{Binary Concrete} : \tilde{e}_{j\zeta} &= \sigma \left(\frac{\ell_{j\zeta} + \log u_{j\zeta}^{\text{ex}} - \log(1 - u_{j\zeta}^{\text{ex}})}{\tau_{\text{ex}}} \right), \\ \text{Gumbel-Softmax} : \tilde{\mathbf{o}}_{j\zeta} &= \text{softmax} \left(\frac{\mathbf{a}_{j\zeta}^{\text{op}} + \mathbf{g}_{j\zeta}^{\text{op}}}{\tau_{\text{op}}} \right), \\ \tilde{\mathbf{h}}_{j\zeta} &= \text{softmax} \left(\frac{\mathbf{a}_{j\zeta}^{\text{ft}} + \mathbf{g}_{j\zeta}^{\text{ft}}}{\tau_{\text{ft}}} \right), \end{aligned} \quad (12)$$

where $\sigma(\cdot)$ is the sigmoid function, $u_{j\zeta}^{\text{ex}} \sim \text{Unif}(0, 1)$, $\mathbf{g}_{j\zeta}^{\text{op}} = \{-\log(-\log u_{j\zeta,r}^{\text{op}})\}_{r=1}^{|\mathcal{O}|}$, $\mathbf{g}_{j\zeta}^{\text{ft}} = \{-\log(-\log u_{j\zeta,k}^{\text{ft}})\}_{k=1}^p$, $u_{j\zeta,r}^{\text{op}} \sim \text{Unif}(0, 1)$, and $u_{j\zeta,k}^{\text{ft}} \sim \text{Unif}(0, 1)$. Also, all uniform random variables are mutually independent. Observe that, $\tilde{e}_{j\zeta} \in \mathbb{R}$, $\tilde{\mathbf{o}}_{j\zeta} \in \mathbb{R}^{|\mathcal{O}|}$, and $\tilde{\mathbf{h}}_{j\zeta} \in \mathbb{R}^p$ can be interpreted as the *soft one-hot encoding* of the corresponding original discrete structural variables. In (12), $(\tau_{\text{ex}}, \tau_{\text{op}}, \tau_{\text{ft}})$ are *temperature parameters* controlling the sharpness of the Binary Concrete and Gumbel-Softmax relaxations. Particularly, higher temperatures yield smooth mixtures of structural configurations whereas for smaller temperatures the relaxed variables concentrate toward discrete structures. A careful annealing of these parameters allows for a balance between exploration and structural learning of symbolic expressions.

Evaluation of soft symbolic trees. Given the soft symbolic tree $\mathcal{S}_j^{\text{soft}}$ as discussed above, we now outline the algorithm for its corresponding evaluation at a given feature vector instance $\mathbf{x}_i \in \mathbb{R}^p$. This evaluation is done recursively over the nodes of $\mathcal{S}_j^{\text{soft}}$. For a given node $\zeta \in \mathcal{Z}_D$, the soft terminal (leaf) contribution is computed as a convex

combination of the input features, $\tilde{\mathbf{h}}_{j\zeta}^\top \mathbf{x}_i$, which corresponds to a *soft feature evaluation*. If the node acts as nonterminal (internal), its output is obtained by a weighted mixture of unary and binary operations over its children. Specifically, the *unary contribution* aggregates, $\tilde{o}_{j\zeta,u} \cdot u(\mathcal{S}_j^{\text{soft}}(\mathbf{x}_i; L(\zeta)))$, over $u \in \mathcal{O}_u$, while the *binary contribution* aggregates, $\tilde{o}_{j\zeta,b} \cdot b(\mathcal{S}_j^{\text{soft}}(\mathbf{x}_i; L(\zeta)), \mathcal{S}_j^{\text{soft}}(\mathbf{x}_i; R(\zeta)))$, over $b \in \mathcal{O}_b$. The *complete node evaluation* is then obtained via *soft gating*:

$$\begin{aligned} \mathcal{S}_j^{\text{soft}}(\mathbf{x}_i; \zeta) &= (1 - \tilde{e}_{j\zeta}) \tilde{\mathbf{h}}_{j\zeta}^\top \mathbf{x}_i + \tilde{e}_{j\zeta} \sum_{u \in \mathcal{O}_u} \tilde{o}_{j\zeta,u} \cdot u(\mathcal{S}_j^{\text{soft}}(\mathbf{x}_i; L(\zeta))) \\ &\quad + \tilde{e}_{j\zeta} \sum_{b \in \mathcal{O}_b} \tilde{o}_{j\zeta,b} \cdot b(\mathcal{S}_j^{\text{soft}}(\mathbf{x}_i; L(\zeta)), \mathcal{S}_j^{\text{soft}}(\mathbf{x}_i; R(\zeta))), \end{aligned} \quad (13)$$

thus smoothly interpolating over all possible combinations of operators and features; see `SOFTEVALATNODE` Algorithm C.1 in Appendix C. Consequently, evaluating a soft symbolic tree corresponds to computing $\mathcal{S}_j^{\text{soft}}(\mathbf{x}_i; \zeta)$ from (13) at the root node $\zeta = 0$. Repeating this procedure for the collection of K soft symbolic trees and all observations yields the *soft design matrix*, $\mathbf{T}_{\text{soft}} \in \mathbb{R}^{n \times \bar{K}+1}$, which includes the intercept column; see `SOFTEVAL` Algorithm C.2 in Appendix C.

Stochastic approximation of $\mathcal{L}(\phi)$. The ELBO objective $\mathcal{L}(\phi)$ in (9) involves the analytically intractable term $\mathbb{E}_{q(\phi)}[\log p(\mathbf{y} | \mathbf{T})]$, since \mathbf{T} exhibits nonlinear dependence on the soft symbolic trees. We therefore approximate this term using *Monte Carlo* (MC) sampling from the distribution induced over $\{\tilde{e}_{j\zeta}, \tilde{\mathbf{o}}_{j\zeta}, \tilde{\mathbf{h}}_{j\zeta} : \zeta \in \mathcal{Z}_D\}_{j=1}^K$ in (12), denoted as $\mathcal{P}_\phi^{\text{soft}}$. In particular, consider S MC samples from $\mathcal{P}_\phi^{\text{soft}}$ and invoking the `SOFTEVAL` Algorithm C.2 in Appendix C, we compute the soft design matrices $\mathbf{T}_{\text{soft}}^{(s)}$, and hence $\log p(\mathbf{y} | \mathbf{T}_{\text{soft}}^{(s)})$ using (6), for $s = 1, \dots, S$. Finally, the MC approximation of $\mathcal{L}(\phi)$ is obtained as:

$$\widehat{\mathcal{L}}(\phi) = \frac{1}{S} \sum_{s=1}^S \log p(\mathbf{y} | \mathbf{T}_{\text{soft}}^{(s)}) - \text{KL}(q_\phi(\Theta) \| \Pi(\Theta)), \quad (14)$$

where $\text{KL}(q_\phi(\Theta) \| \Pi(\Theta))$ is given by (10) and (4); see `APPROXELBO` Algorithm D.3 in Appendix D. The stochastic approximation $\widehat{\mathcal{L}}(\phi)$ in (14) is differentiable with respect to the variational parameters collected in ϕ , thus enabling efficient gradient-based optimization.

Black-box optimization. To obtain the optimal variational parameter vector ϕ^* , we maximize $\widehat{\mathcal{L}}(\phi)$ in (14) using *gradient-based black-box* variational inference [Ranganath et al., 2014, Kucukelbir et al., 2017], leveraging *automatic differentiation* [Rall, 1981] to compute $\nabla_\phi \widehat{\mathcal{L}}(\phi)$. The resulting objective is optimized using the `AdamW` optimizer [Loshchilov and Hutter, 2019]. To progressively sharpen the continuous relaxations in (12), we employ an *annealing schedule* which linearly decreases the temperature across iterations, gradually transitioning from smooth structural mixtures to near-discrete symbolic trees over the course of the algorithm; refer to `VaSST` Algorithm E.4 in Appendix E.

Uncertainty quantification via samples of hard symbolic trees. We conclude variational inference for `VaSST` by generating *hard symbolic trees* using ϕ^* . Concretely, for each draw $s = 1, \dots, H$ and each tree $j = 1, \dots, K$, we sample:

$$\hat{e}_{j\zeta}^{(s)} \sim \text{Ber}(\sigma(\ell_{j\zeta}^*)), \quad \hat{o}_{j\zeta}^{(s)} \sim \text{Cat}(\text{softmax}((\mathbf{a}_{j\zeta}^{\text{op}})^*)), \quad \hat{h}_{j\zeta}^{(s)} \sim \text{Cat}(\text{softmax}((\mathbf{a}_{j\zeta}^{\text{ft}})^*)),$$

respectively for all $\zeta \in \mathcal{Z}_D$. This sampling defines a full depth- D hard binary tree skeleton $(\widehat{\mathcal{F}}_j^{(D)})^{(s)}$, which is then deterministically pruned to obtain:

$$\mathcal{F}(\mathbf{E}_j^{(s)}) = \mathbf{p}((\widehat{\mathcal{F}}_j^{(D)})^{(s)}).$$

The expression design matrix $\mathbf{T}^{(s)}$ is computed by evaluating $\mathcal{F}(\mathbf{E}_j^{(s)})$ at instances $\{\mathbf{x}_i\}_{i=1}^n$. Conditioned on $\mathbf{T}^{(s)}$ and \mathbf{y} , the posterior mean estimates:

$$\boldsymbol{\beta}_{\text{PM}}^{(s)} = \mathbb{E}[\boldsymbol{\beta} | \sigma^2, \mathbf{T}^{(s)}, \mathbf{y}], \quad (\sigma_{\text{PM}}^2)^{(s)} = \mathbb{E}[\sigma^2 | \mathbf{T}^{(s)}, \mathbf{y}],$$

are computed using (7). These H samples are then ranked according to the minimum in-sample root mean squared errors (RMSEs), which enables a balance between *uncertainty quantification*, structural learning of symbolic expressions, and predictive power; see Appendix F for `SAMPLEHARD` Algorithm F.5.

5 VaSST in Action

In this section, we empirically evaluate VaSST through simulation studies and a suite of canonical Feynman equations, assessing: (a) structural learning of symbolic expressions, (b) predictive accuracy (out-of-sample RMSE), (c) stability under experimental noise, and (d) computational scalability (runtime in seconds; against Bayesian SR methods). We compare VaSST with state-of-the-art SR modules spanning *machine learning*, *genetic programming*, and *Bayesian* paradigms, including QLattice [Broløs et al., 2021], gplearn [Stephens, 2016], *Distributed Evolutionary Algorithms in Python* (DEAP) [Fortin et al., 2012], *Bayesian Machine Scientist* (BMS) [Guimerà et al., 2020], and *Bayesian Symbolic Regression* (BSR) [Jin et al., 2020]. For all methods, we adopt a 90/10 train-test split; for VaSST, we report the symbolic expression achieving the *minimum* in-sample RMSE among $H = 2000$ sampled hard symbolic trees and the operator set is taken as: $\mathcal{O} = \{+, \times, -, /, \exp, \log, \sin, \cos, ^2\}$. Experimental configurations are detailed in Appendix H.

5.1 Simulation Experiments

We consider two symbolic data-generating mechanisms of varying levels of structural complexity:

$$\mathbf{y} = \mathbf{x}_0^2 - \mathbf{x}_1 + \frac{1}{2}\mathbf{x}_2^2 + \boldsymbol{\epsilon}, \quad (15)$$

$$\mathbf{y} = 6 \sin(\mathbf{x}_0) \cos(\mathbf{x}_1) + \boldsymbol{\epsilon}, \quad (16)$$

where $\mathbf{x}_j \sim \text{Unif}(2j, 2j+1)$ independently for $j = 0, 1, 2$, with sample size $n = 2000$. We study two experimental regimes: (a) a noiseless setting ($\boldsymbol{\epsilon} = \mathbf{0}$) and (b) noisy settings, where $\boldsymbol{\epsilon} \sim \mathcal{N}_n(\mathbf{0}_n, \sigma^2 \mathbf{I}_n)$ with $\sigma^2 \in \{0.1^2, 0.2^2\}$.

Table 1: Symbolic expressions recovered by VaSST ($K = 3$ and $D = 3$) and competing methods in a single run when learning (15) under an added noise level of $\sigma^2 = 0.1^2$.

Method	Symbolic Expression Learned
VaSST	$0.0246 + 0.99\mathbf{x}_0^2 - 1.01\mathbf{x}_1 + 0.61\mathbf{x}_2^2$
BMS	$\frac{\mathbf{x}_2^2}{\tan(a_0^3)^4} + a_0\mathbf{x}_1 + \mathbf{x}_0^{\mathbf{x}_1} $; a_0 is a constant learned by BMS
BSR	$-3.05 + 0.02 \cos\left((\mathbf{x}_0 - \ln(\mathbf{x}_2))^2\right) + 0.50\mathbf{x}_2^2 + 0.59e^{\mathbf{x}_0}$
QLattice	$-1.00\mathbf{x}_1 + 1.03(0.35 - 0.96\mathbf{x}_0)(-1.04\mathbf{x}_0 - 0.34) + 1.03(21.62 - 3.76\mathbf{x}_2)(-0.13\mathbf{x}_2 - 0.73) + 16.64$
gplearn	$\frac{\mathbf{x}_0\mathbf{x}_2(\mathbf{x}_1 - \mathbf{x}_2)}{(0.382\mathbf{x}_2 - 1)(1 + 2\mathbf{x}_0\mathbf{x}_2^2)} + 0.373\mathbf{x}_2^2 + \mathbf{x}_2 + \mathbf{x}_0 - \mathbf{x}_1 - 1 - \frac{\mathbf{x}_0 - \mathbf{x}_2 - \mathbf{x}_0\mathbf{x}_2}{(\mathbf{x}_0^2 + 0.382\mathbf{x}_2 - 1)(\mathbf{x}_1 - 0.438 - 0.382\mathbf{x}_2^2)}$
DEAP	$1.17((\mathbf{x}_0 + 1.41^2) \times (\mathbf{x}_2 - 4.78)) + 2\mathbf{x}_2$

Table 2: Out-of-sample RMSEs (computed on a 10% held-out test set) of VaSST ($K = 3$ and $D = 3$) and competing methods over 10 repetitions (mean \pm standard deviation) for learning (15) across all noise settings.

Noiseless		$\sigma^2 = 0.1^2$		$\sigma^2 = 0.2^2$	
Method	Mean \pm Std. Dev.	Method	Mean \pm Std. Dev.	Method	Mean \pm Std. Dev.
VaSST	0.002925 \pm 0.000661	VaSST	0.100255 \pm 0.001524	VaSST	0.200428 \pm 0.003076
QLattice	0.005195 \pm 0.002953	QLattice	0.101894 \pm 0.002699	QLattice	0.202036 \pm 0.004099
BMS	0.062021 \pm 0.030156	BMS	0.119885 \pm 0.016030	BMS	0.208089 \pm 0.008459
gplearn	0.298429 \pm 0.204293	gplearn	0.322157 \pm 0.188765	gplearn	0.353564 \pm 0.152275
BSR	0.601950 \pm 0.586909	BSR	0.486881 \pm 0.456420	BSR	0.532810 \pm 0.436730
DEAP	0.697424 \pm 0.245698	DEAP	0.724823 \pm 0.259967	DEAP	0.736821 \pm 0.241499

For a representative run under noise level $\sigma^2 = 0.1^2$, Table 1 reports the symbolic expressions recovered by each method when learning (15); additional results for other noise levels are provided in Appendix I.1. VaSST accurately recovers the true structure while fitting $K = 3$ symbolic trees each of maximum depth $D = 3$, whereas competing methods largely fail to identify the underlying symbolic expression across noise levels, instead producing substantially more complicated expressions. When learning the simpler trigonometric expression in (16), results across noise levels are summarized in Appendix I.1. Here, VaSST ($K = 3$ and $D = 3$) again identifies the correct symbolic structure, alongside BMS. In contrast, BSR, QLattice, gplearn, and DEAP tend to generate unnecessarily complex output expressions. Notably, the structural recovery of VaSST (for both (15) and (16)) and of BMS (for the simpler model in (16)) remains consistent across increasing noise levels, reflecting stability of the learned symbolic structures under observational perturbations.

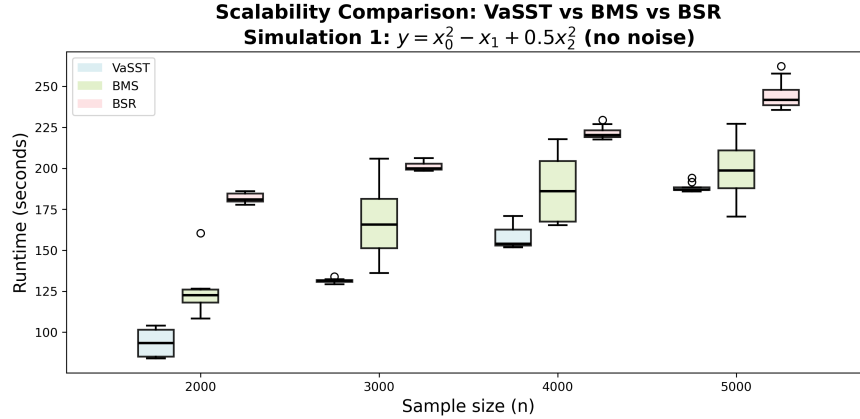


Figure 3: Computational scalability of VaSST, BMS, BSR.

VaSST effectively balances structural learning and predictive accuracy, achieving consistently low out-of-sample RMSEs across all noise levels when learning (15) (Table 2; see also Figure I.1 in Appendix I.2). Similar behavior is observed for (16) in Appendix I.2. Although BMS and QLattice perform competitively for the simpler model, QLattice (in general for both (15) and (16)) and BMS (for higher structural complexity as in (15)) frequently produce overly complex expressions indicative of overfitting, whereas VaSST outperforms by attaining the strongest predictive accuracy while maintaining structural parsimony. This structural parsimony is driven by the depth-adaptive split probability in (3), which penalizes unnecessarily complex expressions and consequently downweights them through small posterior mean estimates of β .

Furthermore, in learning (15) with no noise, Figure 3 highlights the computational scalability of VaSST relative to other Bayesian modules, i.e., BMS and BSR (maintained at similar configurations to that of VaSST for fair comparison). For increasing sample sizes $n \in \{2000, 3000, 4000, 5000\}$ with 10 repetitions per n , VaSST invariably records the lowest compute runtime, demonstrating superior scalability.

To quantify uncertainty over the learned symbolic tree structures for both (15) and (16) across all noise levels, we report in Appendix I.3 the top 5 symbolic expressions obtained from $H = 2000$ sampled hard symbolic trees under VaSST ($K = 3$ and $D = 3$), ranked according to their minimum in-sample RMSE.

5.2 Application to Feynman Equations

We evaluate VaSST on benchmark SR problems from the *Feynman Symbolic Regression Database* (FSReD) [Udrescu and Tegmark, 2020] within SRBench, which contains over 100 equations from the Feynman Lectures on Physics [Feynman et al., 2015] with 10^5 observations per equation. We consider four representative laws spanning electromagnetism, gravitation, and heat transfer with varying symbolic complexity, i.e., Coulomb’s law (**CL**), the change in gravitational potential energy (**CPE**), the Lorentz force on a moving charge in an electromagnetic field (**FCE**), and Fourier’s law of thermal conduction (**FTC**):

$$\begin{aligned} \mathbf{CL} : F &= 0.08 \frac{q_1 q_2}{\epsilon r^2}, \quad \mathbf{CPE} : \Delta U = G m_1 m_2 \left(\frac{1}{r_2} - \frac{1}{r_1} \right), \\ \mathbf{FCE} : F &= q (E_f + v B \sin \theta), \quad \mathbf{FTC} : P = \frac{\kappa A (T_2 - T_1)}{d}, \end{aligned}$$

where the input features, responses, and constants are described in Appendix J. For each equation, we randomly subsample $n = 2000$ observations. We consider three noise regimes: the original dataset (noiseless) and two settings with additive Gaussian noise of variance $\sigma^2 \in \{0.1^2, 0.2^2\}$ applied to the response variable to mimic measurement error and/or experimental perturbations. In all experiments VaSST fits $K = 3$ symbolic trees each of maximum depth $D = 3$.

Across all equation datasets and noise levels, the minimum RMSE model produced by VaSST recovers the correct symbolic expression. Among competing methods, BMS performs well for **CL**, **CPE**, and **FCE** across all noise levels but encounters numerical errors for **FTC**. The genetic programming module `gplearn` successfully identifies the correct expression in all but the more complex **FCE** case, where it yields unnecessarily complicated forms. The neural network-based QLattice fails to recover the true expressions in most cases and instead produces highly complex formulas, except for the relatively simple **CL**. Similarly, BSR and DEAP consistently favor overly complex symbolic expressions and do not recover the ground-truth equations. Table 3 summarizes symbolic recovery across all methods.

As a representative example, Table 4 reports the expressions learned by each method for **FTC** at $\sigma^2 = 0.1^2$, while the remaining results are provided in Appendix K.1.

Table 3: Exact symbolic recovery for the Feynman equations. \checkmark and \times denote success and failure, respectively; symbols in each cell correspond to noiseless, $\sigma^2 = 0.1^2$, $\sigma^2 = 0.2^2$.

Method	CL	CPE	FCE	FTC
VaSST	$\checkmark\checkmark\checkmark$	$\checkmark\checkmark\checkmark$	$\checkmark\checkmark\checkmark$	$\checkmark\checkmark\checkmark$
BMS	$\checkmark\checkmark\checkmark$	$\checkmark\checkmark\checkmark$	$\checkmark\checkmark\checkmark$	$\times\times\times$
BSR	$\times\times\times$	$\times\times\times$	$\times\times\times$	$\times\times\times$
DEAP	$\times\times\times$	$\times\times\times$	$\times\times\times$	$\times\times\times$
gplearn	$\checkmark\checkmark\checkmark$	$\checkmark\checkmark\checkmark$	$\times\times\times$	$\checkmark\checkmark\checkmark$
QLattice	$\checkmark\checkmark\checkmark$	$\times\times\times$	$\times\times\times$	$\checkmark\times\times$

Table 4: Symbolic expressions recovered by VaSST ($K = 3$ and $D = 3$) and competing methods for **FTC**: $P = \kappa A(T_2 - T_1)d^{-1}$ under $\sigma^2 = 0.1^2$. Out-of-sample RMSE is evaluated on a 10% held-out test set, with all coefficients in the symbolic expression reported up to three decimal places across all methods.

Method	Symbolic Expression Learned	RMSE
VaSST	$0.002 - 0.943 \frac{\kappa A T_1}{d} + 1.006 \frac{\kappa A T_2}{d}$	1.00325×10^{-1}
BMS	BMS failed to return valid expression	–
BSR	$0.805 - 0.103 \exp\left(\cos\left(\frac{d}{\sqrt{A}}\right)\right) + 0.150 \kappa^2 A T_1^2$	4.06545×10^{-1}
QLattice	$(0.469 - 0.518 \frac{T_2}{T_1})(\kappa\sqrt{A}T_1 + 0.075) \exp\left(-0.183 \frac{d}{\sqrt{A}}\right) - 0.033$	1.01498×10^{-1}
gplearn	$\frac{\kappa A (T_2 - T_1)}{d}$	1.00224×10^{-1}
DEAP	$\kappa\sqrt{A}T_2^6 T_1^{-5} \left[\kappa\sqrt{A}T_1 - 4.828 \left(1 + \frac{T_2}{T_1}\right) + \frac{d}{\sqrt{A}} \left(-\left(\frac{T_2}{T_1}\right)^2 + \left(\frac{T_2}{T_1}\right)^3 + \left(\frac{T_2}{T_1}\right)^4 + \left(\frac{T_2}{T_1}\right)^5 \right) \right]^{-1}$	1.00126×10^{-1}

In terms of predictive performance, measured using out-of-sample RMSE, VaSST is consistently among the top-performing methods, typically alongside BMS, except for **FTC** where BMS fails due to numerical issues. Genetic programming-based gplearn and DEAP, and neural network-based QLattice often achieve competitive prediction accuracy but only through substantially more complex symbolic expressions. Lastly, BSR yields consistently higher prediction errors. A full comparison of out-of-sample RMSE values is provided in Appendix K.2.

Additionally, VaSST exhibits substantially faster runtimes than the Bayesian SR methods BMS and BSR across all Feynman equation datasets and noise settings, highlighting the computational advantages of the proposed variational inference framework. Detailed runtime comparisons are reported in Appendix K.3.

Finally, beyond competitive performance in prediction and structural learning, VaSST provides uncertainty quantification in symbolic equation discovery by producing multiple candidate symbolic ensembles ranked by minimum in-sample RMSE. The top 5 expressions across all Feynman equations and noise levels are reported in Appendix K.4.

6 Conclusion

We presented VaSST, a fully probabilistic framework for SR that leverages variational inference with continuous relaxations of symbolic trees. It enables scalable gradient-based optimization while preserving interpretability equipped with principled uncertainty quantification. Empirically, VaSST achieves strong structural recovery, competitive predictive accuracy, stability under noise, and notable computational gains over existing Bayesian SR methods.

This work opens promising future avenues for fully probabilistic and scalable variational inference-based SR, including the development of more structured optimization strategies for the variational objective to further enhance scalability relative to modern machine learning-based approaches.

References

- Shankar Bhamidi, Guy Bresler, and Allan Sly. Mixing time of exponential random graphs. In *49th Annual IEEE Symposium on Foundations of Computer Science*, pages 803–812, 2008.
- David M. Blei, Andrew Y. Ng, and Michael I. Jordan. Latent dirichlet allocation. *Journal of Machine Learning Research*, 3:993–1022, 2003.
- David M. Blei, Alp Kucukelbir, and Jon D. McAuliffe. Variational Inference: A Review for Statisticians. *Journal of the American Statistical Association*, 112(518):859–877, 2017.
- Frimpong Boadu, Ahhyun Lee, and Jianlin Cheng. Deep learning methods for protein function prediction. *PROTEOMICS*, 25(1-2):2300471, 2025.
- Leo Breiman. Bagging predictors. *Machine Learning*, 24(2):123–140, 1996.
- Leo Breiman, Jerome Friedman, R. A. Olshen, and Charles J. Stone. *Classification and Regression Trees (1st ed.)*. Chapman and Hall/CRC, 1984.
- Kevin Broløs, Meera Vieira René, Machado, Chris Cave, Jaan Kasak, Valdemar Stentoft-Hansen, Victor Galindo Batanero, Tom Jelen, and Casper Wilstrup. An approach to symbolic regression using feyn. *arXiv:2104.05417*, 2021.
- Steven L. Brunton, Joshua L. Proctor, and J. Nathan Kutz. Discovering governing equations from data by sparse identification of nonlinear dynamical systems. *Proceedings of the National Academy of Sciences*, 113(15):3932–3937, 2016.
- Keith T Butler, Daniel W Davies, Hugh Cartwright, Olexandr Isayev, and Aron Walsh. Machine learning for molecular and materials science. *Nature*, 559(7715):547–555, 2018.
- Hugh A. Chipman, Edward I. George, and Robert E. McCulloch. Bayesian CART Model Search. *Journal of the American Statistical Association*, 93(443):935–948, 1998.
- Hugh A. Chipman, Edward I. George, and Robert E. McCulloch. BART: Bayesian additive regression trees. *The Annals of Applied Statistics*, 4(1):266–298, 2010.
- J. W. Davidson, D. A. Savic, and G. A. Walters. Symbolic and numerical regression: experiments and applications. *Information Sciences*, 150(1–2):95–117, 2003.
- David G. T. Dension, Bani K. Mallick, and Adrian F. M. Smith. A Bayesian CART algorithm. *Biometrika*, 85(2):363–377, 1998.
- R.P. Feynman, R.B. Leighton, and M. Sands. *The Feynman Lectures on Physics, Vol. I: The New Millennium Edition: Mainly Mechanics, Radiation, and Heat*. Number v. 1. Basic Books, 2015.
- Félix-Antoine Fortin, François-Michel De Rainville, Marc-André Gardner, Marc Parizeau, and Christian Gagné. DEAP: Evolutionary algorithms made easy. *Journal of Machine Learning Research*, 13(70):2171–2175, 2012.
- Ryan Giordano, Martin Ingram, and Tamara Broderick. Black box variational inference with a deterministic objective: Faster, more accurate, and even more black box. *Journal of Machine Learning Research*, 25(18):1–39, 2024.
- Alex Graves. Practical Variational Inference for Neural Networks. In *Advances in Neural Information Processing Systems*, volume 24, 2011.
- Roger Guimerà, Ignasi Reichardt, Antoni Aguilar-Mogas, Francesco A Massucci, Manuel Miranda, Jordi Pallarès, and Marta Sales-Pardo. A bayesian machine scientist to aid in the solution of challenging scientific problems. *Science advances*, 6(5):eaav6971, 2020.
- Eric Jang, Shixiang Gu, and Ben Poole. Categorical reparameterization with gumbel-softmax. *arXiv:1611.01144*, 2016.
- William H. Jefferys and James O. Berger. Ockham’s Razor and Bayesian Analysis. *American Scientist*, 80(1):64–72, 1992. ISSN 00030996.
- Ying Jin, Weilin Fu, Jian Kang, Jiadong Guo, and Jian Guo. Bayesian Symbolic Regression. *arXiv:1910.08892*, 2020.
- Michael I Jordan, Zoubin Ghahramani, Tommi S Jaakkola, and Lawrence K Saul. An introduction to variational methods for graphical models. *Machine learning*, 37(2):183–233, 1999.
- Pierre-Alexandre Kamienny, Stéphane d’Ascoli, Guillaume Lample, and François Charton. End-to-end symbolic regression with transformers. In *Advances in Neural Information Processing Systems*, 2022.
- Michael F. Korn. Accuracy in symbolic regression. In *Genetic Programming Theory and Practice IX*, pages 129–151. 2011.
- John R Koza. Genetic programming as a means for programming computers by natural selection. *Statistics and computing*, 4(2):87–112, 1994.

- Alp Kucukelbir, Dustin Tran, Rajesh Ranganath, Andrew Gelman, and David M Blei. Automatic differentiation variational inference. *Journal of machine learning research*, 18(14):1–45, 2017.
- Krzysztof Łatuszyński, Matthew T Moores, and Timothée Stumpf-Fétizon. MCMC for multi-modal distributions. *arXiv:2501.05908*, 2025.
- Hanxiao Liu, Karen Simonyan, and Yiming Yang. DARTS: Differentiable architecture search. In *International Conference on Learning Representations*, 2019.
- Ilya Loshchilov and Frank Hutter. Decoupled Weight Decay Regularization. In *International Conference on Learning Representations*, 2019.
- Chris J. Maddison, Andriy Mnih, and Yee Whye Teh. The concrete distribution: A continuous relaxation of discrete random variables. *arXiv:1611.00712*, 2017.
- Brenden K Petersen, Mikel Landajuela Larma, Terrell N. Mundhenk, Claudio Prata Santiago, Soo Kyung Kim, and Joanne Taery Kim. Deep symbolic regression: Recovering mathematical expressions from data via risk-seeking policy gradients. In *International Conference on Learning Representations*, 2021.
- M. Raissi, P. Perdikaris, and G.E. Karniadakis. Physics-informed neural networks: A deep learning framework for solving forward and inverse problems involving nonlinear partial differential equations. *Journal of Computational Physics*, 378:686–707, 2019.
- Louis B Rall. *Automatic differentiation: Techniques and applications*. Springer, 1981.
- Rajesh Ranganath, Sean Gerrish, and David M. Blei. Black Box Variational Inference. In *International Conference on Artificial Intelligence and Statistics*, volume 33, pages 814–822, 2014.
- Carl Edward Rasmussen and Christopher K. I. Williams. *Gaussian Processes for Machine Learning*. MIT Press, 2006.
- Sebastian Salazar. VaRT: Variational regression trees. In *Advances in Neural Information Processing Systems*, 2023.
- Michael Schmidt and Hod Lipson. Distilling free-form natural laws from experimental data. *Science*, 324(5923):81–85, 2009.
- Trevor Stephens. gplearn: Genetic Programming in Python, 2016. URL <https://github.com/trevorstephens/gplearn>.
- Robert Tibshirani. Regression Shrinkage and Selection via the Lasso. *Journal of the Royal Statistical Society. Series B (Methodological)*, 58(1):267–288, 1996.
- Silviu-Marian Udrescu and Max Tegmark. AI Feynman: A physics-inspired method for symbolic regression. *Science Advances*, 6(16):eaay2631, 2020.
- Marco Virgolin and Solon P. Pissis. Symbolic regression is np-hard. In *Proceedings of the Genetic and Evolutionary Computation Conference*, 2022.
- Martin J. Wainwright and Michael I. Jordan. Graphical Models, Exponential Families, and Variational Inference. *Foundations and Trends in Machine Learning*, 1(1–2):1–305, 2008.
- Guanjie Wang, Erpeng Wang, Zefeng Li, Jian Zhou, and Zhimei Sun. Exploring the mathematic equations behind the materials science data using interpretable symbolic regression. *Interdisciplinary Materials*, 3(5):637–657, 2024.
- Ronald J Williams. Simple statistical gradient-following algorithms for connectionist reinforcement learning. *Machine learning*, 8(3):229–256, 1992.
- Huijun Zhang, Yaxin Liu, Chongyu Zhang, and Ningyun Li. Machine Learning Methods for Weather Forecasting: A Survey. *Atmosphere*, 16(1), 2025.

Supplementary Materials for VaSST: Variational Inference for Symbolic Regression using Soft Symbolic Trees

A Notations

Table A.1: Special functions and other notations.

Symbol	Name	Definition
\mathbb{N}	Natural numbers	Set $\{1, 2, 3, \dots\}$
\mathbb{R}	Real numbers	Set of real numbers
\mathbb{R}^p	p -dimensional Euclidean space	$\{\mathbf{x} = (x_1, \dots, x_p)^\top : x_i \in \mathbb{R}\}$
$\mathbb{R}^{m \times n}$	Real matrix space	Space of real $m \times n$ matrices
$ A $	Cardinality	Number of elements in a finite set A
$\Gamma(t)$	Gamma function	$\Gamma(t) = \int_0^\infty x^{t-1} e^{-x} dx$
$\Psi(t)$	Digamma function	$\Psi(t) = \frac{d}{dt} \log \Gamma(t)$
$\mathcal{B}(\boldsymbol{\eta})$	Multivariate Beta function	$\mathcal{B}(\boldsymbol{\eta}) = \frac{\prod_{k=1}^m \Gamma(\eta_k)}{\Gamma(\sum_{k=1}^m \eta_k)}$
$\mathbf{1}_m$	Vector of ones	$(1, \dots, 1)^\top \in \mathbb{R}^m$
$\mathbf{0}_m$	Vector of zeros	$(0, \dots, 0)^\top \in \mathbb{R}^m$
\mathbf{I}_m	Identity matrix of order m	$(\mathbf{I}_m)_{ij} = \mathbf{1}\{i = j\}, \quad i, j = 1, \dots, m$
$ \mathbf{A} $	Determinant	Determinant of the matrix $\mathbf{A} \in \mathbb{R}^{m \times m}$
Δ^m	m -dimensional simplex	$\{\mathbf{w} \in [0, \infty)^m : \mathbf{1}_m^\top \mathbf{w} = 1\}$
$\mathcal{O}(g(n))$	Order notation	$f(n) = \mathcal{O}(g(n))$ if $ f(n) \leq C g(n) $ for some constant $C > 0$ and sufficiently large n

B Parameterization Details of Distribution Families used in VaSST

The VaSST framework utilizes several standard probability distributions for model specification and prior construction. Although these distributions are widely used in the machine learning literature, multiple parameterizations are common for some of them across various sources. For clarity and reproducibility, we explicitly document the notation and parameterizations adopted in this work.

Normal Inverse-Gamma. We use the conjugate Normal Inverse-Gamma (NIG) prior for Gaussian linear regression parameters:

$$\boldsymbol{\beta} \mid \sigma^2 \sim N_d(\boldsymbol{\mu}_0, \sigma^2 \boldsymbol{\Sigma}_0), \quad \sigma^2 \sim \text{IG}(a_0, b_0), \quad (\text{B.1})$$

where $d = K + 1$, $\boldsymbol{\mu}_0 \in \mathbb{R}^d$, $\boldsymbol{\Sigma}_0 \in \mathbb{R}^{d \times d}$ is symmetric positive definite, and $a_0, b_0 > 0$. Our Inverse-Gamma parameterization, i.e., $\text{IG}(a, b)$, uses the density:

$$\Pi(\sigma^2) = \frac{b^a}{\Gamma(a)} (\sigma^2)^{-(a+1)} \exp\left(-\frac{b}{\sigma^2}\right), \quad \sigma^2 > 0, \quad (\text{B.2})$$

where $\Gamma(\cdot)$ is the Gamma function in Table A.1. The conditional Gaussian density in (B.1) is:

$$\Pi(\boldsymbol{\beta} \mid \sigma^2) = (2\pi)^{-\frac{d}{2}} (\sigma^2)^{-\frac{d}{2}} |\boldsymbol{\Sigma}_0|^{-\frac{1}{2}} \exp\left\{-\frac{1}{2\sigma^2} (\boldsymbol{\beta} - \boldsymbol{\mu}_0)^\top \boldsymbol{\Sigma}_0^{-1} (\boldsymbol{\beta} - \boldsymbol{\mu}_0)\right\}. \quad (\text{B.3})$$

Equivalently, the joint prior is $\Pi(\boldsymbol{\beta}, \sigma^2) = \Pi(\boldsymbol{\beta} \mid \sigma^2)\Pi(\sigma^2)$.

Bernoulli. A Bernoulli random variable $E \sim \text{Ber}(p)$, with $p \in (0, 1)$, has support $\{0, 1\}$ and probability mass function:

$$\Pi(e) = p^e (1-p)^{1-e}, \quad e \in \{0, 1\}. \quad (\text{B.4})$$

In our tree prior, the expansion indicator follows $e_{j\zeta} \sim \text{Ber}(p_\zeta)$ with $p_\zeta = \alpha(1 + d_\zeta)^{-\delta}$, where $\alpha \in (0, 1)$ and $\delta > 0$.

Dirichlet. For $m \geq 2$, a vector $\mathbf{w} \in \Delta^m$ follows a Dirichlet distribution with concentration vector $\boldsymbol{\eta} = (\eta_1, \dots, \eta_m)^\top \in (0, \infty)^m$, i.e., $\mathbf{w} \sim \text{Dir}(\boldsymbol{\eta})$, having density:

$$p(\mathbf{w} \mid \boldsymbol{\eta}) = \frac{1}{\mathcal{B}(\boldsymbol{\eta})} \prod_{k=1}^m w_k^{\eta_k - 1}, \quad \mathbf{w} \in \Delta^m, \quad (\text{B.5})$$

where $\mathcal{B}(\cdot)$ is the multivariate Beta function and Δ^m is the m -dimensional simplex, as defined in Table A.1. In VaSST, the operator and feature weight vectors follow $\mathbf{w}_{\text{op}} \sim \text{Dir}(\boldsymbol{\eta}_{\text{op}})$ and $\mathbf{w}_{\text{ft}} \sim \text{Dir}(\boldsymbol{\eta}_{\text{ft}})$, where $\mathbf{w}_{\text{op}} \in \Delta^{|\mathcal{O}|}$ and $\mathbf{w}_{\text{ft}} \in \Delta^p$, respectively.

Categorical. Let $\mathbf{w} \in \Delta^m$. A Categorical random variable, $c \sim \text{Cat}(\mathbf{w})$, takes values in $\{1, \dots, m\}$ with probability mass function:

$$\Pi(c = j \mid \mathbf{w}) = w_j, \quad j \in \{1, \dots, m\} \quad (\text{B.6})$$

In VaSST, conditional on weights, we assign operators and features via

$$o_{j\zeta} \mid \mathbf{w}_{\text{op}} \sim \text{Cat}(\mathbf{w}_{\text{op}}), \quad h_{j\zeta} \mid \mathbf{w}_{\text{ft}} \sim \text{Cat}(\mathbf{w}_{\text{ft}}), \quad o_{j\zeta} \in \mathcal{O}, \quad h_{j\zeta} \in \mathcal{X}. \quad (\text{B.7})$$

When needed, we identify \mathcal{O} and \mathcal{X} with index sets of sizes $|\mathcal{O}|$ and p , respectively, so that (B.6) applies directly.

Uniform. A continuous random variable $u \sim \text{Unif}(a, b)$, with $a < b$, has support on the interval (a, b) and probability density function:

$$\Pi(u) = \frac{1}{b-a}, \quad a < u < b, \quad (\text{B.8})$$

and $\Pi(u) = 0$ otherwise. In the Binary Concrete and Gumbel-Softmax continuous relaxations in Section 4, the $\text{Unif}(0, 1)$ distribution was used to reparameterize the discrete structural variables. Further, in simulation experiments in Section 5.1, uniform distributions were used to generate the input variables.

C Soft Evaluation Algorithms

C.1 Soft Evaluation At a Node

Algorithm C.1: The $\text{SOFT EVAL AT NODE}(\zeta', \mathbf{x}_i, j, \mathcal{O}, \{\tilde{e}_{j\zeta}, \tilde{\mathbf{o}}_{j\zeta}, \tilde{\mathbf{h}}_{j\zeta} : \zeta \in \mathcal{Z}_D\})$ algorithm for evaluating a soft symbolic subtree rooted at a given node ζ' .

Input: A given node: ζ' ; feature vector: $\mathbf{x}_i \in \mathbb{R}^p$; soft symbolic tree index: $j \in \{1, \dots, K\}$; the operator set: $\mathcal{O} = \mathcal{O}_u \cup \mathcal{O}_b$; soft relaxations: $\{\tilde{e}_{j\zeta}, \tilde{\mathbf{o}}_{j\zeta}, \tilde{\mathbf{h}}_{j\zeta} : \zeta \in \mathcal{Z}_D\}$.

Output: $\mathcal{S}_j^{\text{soft}}(\mathbf{x}_i; \zeta') \in \mathbb{R}$.

// Soft feature evaluation

Term(\mathbf{x}_i, j, ζ') $\leftarrow \tilde{\mathbf{h}}_{j\zeta'}^\top \mathbf{x}_i$

// Soft operator evaluation

// $L(\zeta')$ and $R(\zeta')$ are the left and right children of ζ' , respectively

NontermUnary(\mathbf{x}_i, j, ζ') $\leftarrow \sum_{u \in \mathcal{O}_u} \tilde{o}_{j\zeta', u} \cdot u(\mathcal{S}_j^{\text{soft}}(\mathbf{x}_i; L(\zeta')))$

NontermBinary(\mathbf{x}_i, j, ζ') $\leftarrow \sum_{b \in \mathcal{O}_b} \tilde{o}_{j\zeta', b} \cdot b(\mathcal{S}_j^{\text{soft}}(\mathbf{x}_i; L(\zeta')), \mathcal{S}_j^{\text{soft}}(\mathbf{x}_i; R(\zeta')))$

Nonterm(\mathbf{x}_i, j, ζ') $\leftarrow \text{NontermUnary}(\mathbf{x}_i, j, \zeta') + \text{NontermBinary}(\mathbf{x}_i, j, \zeta')$

// Complete soft evaluation at ζ'

$\mathcal{S}_j^{\text{soft}}(\mathbf{x}_i; \zeta') \leftarrow \tilde{e}_{j\zeta'} \text{Nonterm}(\mathbf{x}_i, j, \zeta') + (1 - \tilde{e}_{j\zeta'}) \text{Term}(\mathbf{x}_i, j, \zeta')$

return $\mathcal{S}_j^{\text{soft}}(\mathbf{x}_i; \zeta')$

C.2 Complete Soft Evaluation

Algorithm C.2: The $\text{SOFT EVAL}(\{\mathbf{x}_i \in \mathbb{R}^p : i = 1, \dots, n\}, \mathcal{O}, \{\tilde{e}_{j\zeta}, \tilde{\mathbf{o}}_{j\zeta}, \tilde{\mathbf{h}}_{j\zeta} : \zeta \in \mathcal{Z}_D\}_{j=1}^K)$ algorithm for evaluating an ensemble of K soft symbolic trees.

Input: Feature vectors: $\{\mathbf{x}_i \in \mathbb{R}^p : i = 1, \dots, n\}$; the operator set: $\mathcal{O} = \mathcal{O}_u \cup \mathcal{O}_b$; soft relaxations: $\{\tilde{e}_{j\zeta}, \tilde{\mathbf{o}}_{j\zeta}, \tilde{\mathbf{h}}_{j\zeta} : \zeta \in \mathcal{Z}_D\}_{j=1}^K$.

Output: $\mathbf{T}_{\text{soft}} \in \mathbb{R}^{n \times \overline{K+1}}$.

for $i \leftarrow 1$ **to** n **do**

// Intercept term set to 1

$t_{i0} \leftarrow 1$

for $j \leftarrow 1$ **to** K **do**

// j th soft symbolic tree evaluated at root node for \mathbf{x}_i

$t_{ij} = \mathcal{S}_j^{\text{soft}}(\mathbf{x}_i; \zeta' = 0)$ from Algorithm C.1: SOFT EVAL AT NODE

$\mathbf{T}_{\text{soft}} \leftarrow (t_{ij})_{1 \leq i \leq n, 0 \leq j \leq K}$

return \mathbf{T}_{soft}

D Algorithm for Approximation of $\mathcal{L}(\phi)$

Algorithm D.3: The APPROXELBO($\mathcal{D}_n, (\boldsymbol{\mu}_0, \boldsymbol{\Sigma}_0, a_0, b_0, \boldsymbol{\eta}_{\text{op}}, \boldsymbol{\eta}_{\text{ft}}, \boldsymbol{\alpha}, \boldsymbol{\delta}), \mathcal{O}, \phi, (\tau_{\text{ex}}, \tau_{\text{op}}, \tau_{\text{ft}}), S$) algorithm for computing Monte Carlo approximation of $\mathcal{L}(\phi)$.

Input: Data: $\mathcal{D}_n = \{(\mathbf{x}_i, y_i) : i = 1, \dots, n\}$; full set of prior hyperparameters: $(\boldsymbol{\mu}_0, \boldsymbol{\Sigma}_0, a_0, b_0, \boldsymbol{\eta}_{\text{op}}, \boldsymbol{\eta}_{\text{ft}}, \boldsymbol{\alpha}, \boldsymbol{\delta})$; the operator set: $\mathcal{O} = \mathcal{O}_u \cup \mathcal{O}_b$; the variational parameter vector: ϕ ; the temperature parameters: $(\tau_{\text{ex}}, \tau_{\text{op}}, \tau_{\text{ft}})$; the Monte Carlo sample size: S .

Output: $\widehat{\mathcal{L}}(\phi)$.

// Compute the Kullback-Leibler term

$\mathcal{H} \leftarrow \text{KL}(q_\phi(\Theta) \parallel \Pi(\Theta))$, using (10)

for $s \leftarrow 1$ **to** S **do**

// Sample soft tree structural parameters from $\mathcal{P}_\phi^{\text{soft}}$

$\{\tilde{e}_{j\zeta}^{(s)}, \tilde{\mathbf{o}}_{j\zeta}^{(s)}, \tilde{\mathbf{h}}_{j\zeta}^{(s)} : \zeta \in \mathcal{L}_D\}_{j=1}^K \sim \mathcal{P}_\phi^{\text{soft}}$, using the temperature parameters

// Computing soft symbolic design matrix

$\mathbf{T}_{\text{soft}}^{(s)} \leftarrow \text{SOFTEVAL}(\{\mathbf{x}_i \in \mathbb{R}^p : i = 1, \dots, n\}, \mathcal{O}, \{\tilde{e}_{j\zeta}^{(s)}, \tilde{\mathbf{o}}_{j\zeta}^{(s)}, \tilde{\mathbf{h}}_{j\zeta}^{(s)} : \zeta \in \mathcal{L}_D\}_{j=1}^K)$

// Computing the marginal likelihood at $\mathbf{T}_{\text{soft}}^{(s)}$

$\text{ML}^{(s)} \leftarrow \log p(\mathbf{y} \mid \mathbf{T}_{\text{soft}}^{(s)})$, using (6)

$\widehat{\mathcal{L}}(\phi) \leftarrow \frac{1}{S} \sum_{s=1}^S \text{ML}^{(s)} - \mathcal{H}$

return $\widehat{\mathcal{L}}(\phi)$

E The VaSST Algorithm

Algorithm E.4: The VaSST($\mathcal{D}_n, (\boldsymbol{\mu}_0, \boldsymbol{\Sigma}_0, a_0, b_0, \boldsymbol{\eta}_{\text{op}}, \boldsymbol{\eta}_{\text{ft}}, \alpha, \delta), \mathcal{O}, \phi^{\text{init}}, T, (\tau_{\text{start}}, \tau_{\text{end}}, T_\tau), S, \gamma, c$) algorithm for symbolic regression using automatic differentiation-based black-box variational inference

Input: Data: $\mathcal{D}_n = \{(\mathbf{x}_i, y_i) : i = 1, \dots, n\}$; full set of prior hyperparameters: $(\boldsymbol{\mu}_0, \boldsymbol{\Sigma}_0, a_0, b_0, \boldsymbol{\eta}_{\text{op}}, \boldsymbol{\eta}_{\text{ft}}, \alpha, \delta)$; the operator set: $\mathcal{O} = \mathcal{O}_u \cup \mathcal{O}_b$; initial variational parameter vector: ϕ^{init} ; number of steps: T ; temperature schedule: $(\tau_{\text{start}}, \tau_{\text{end}}, T_\tau)$; Monte Carlo sample size: S ; learning rate: γ ; gradient clipping threshold: c .

Output: Optimized variational parameter vector ϕ^* .

Set $\phi_0 \leftarrow \phi^{\text{init}}$

Initialize AdamW optimizer with learning rate γ

for $t \leftarrow 1$ **to** T **do**

 // Anneal temperature parameters

$\tau_t \leftarrow \tau_{\text{start}} + (\tau_{\text{end}} - \tau_{\text{start}}) \cdot \min\{\frac{t}{T_\tau}, 1\}$

 Set $(\tau_{\text{ex}}, \tau_{\text{op}}, \tau_{\text{ft}}) \leftarrow (\tau_t, \tau_t, \tau_t)$

 Set all gradients to zero

 // Compute stochastic ELBO estimate

$\widehat{\mathcal{L}}(\phi) \leftarrow \text{APPROXELBO}(\mathcal{D}_n, (\boldsymbol{\mu}_0, \boldsymbol{\Sigma}_0, a_0, b_0, \boldsymbol{\eta}_{\text{op}}, \boldsymbol{\eta}_{\text{ft}}, \alpha, \delta), \mathcal{O}, \phi, (\tau_{\text{ex}}, \tau_{\text{op}}, \tau_{\text{ft}}), S)$

$\mathcal{J} \leftarrow -\widehat{\mathcal{L}}(\phi)$

 // minimize negative objective

if \mathcal{J} is not finite **then**

 | **continue**

 Backpropagate: compute $\nabla_\phi \mathcal{J}$

if any component of $\nabla_\phi \mathcal{J}$ is not finite **then**

 | Set all gradients to zero; **continue**

 Clip gradients: $\|\nabla_\phi \mathcal{J}\| \leq c$

$\phi_t \leftarrow$ AdamW update step on ϕ

Set $\phi^* \leftarrow \phi_T$

return ϕ^*

F Algorithm for Sampling Hard Symbolic Trees

Algorithm F.5: The `SAMPLEHARD`($\mathcal{D}_n, (\boldsymbol{\mu}_0, \boldsymbol{\Sigma}_0, a_0, b_0, \boldsymbol{\eta}_{\text{op}}, \boldsymbol{\eta}_{\text{ft}}, \alpha, \delta), \phi^*, \mathcal{O}, H$) algorithm to draw samples of hard symbolic trees from learned soft structural representations

Input: Data: $\mathcal{D}_n = \{(\mathbf{x}_i, y_i) : i = 1, \dots, n\}$; full set of prior hyperparameters: $(\boldsymbol{\mu}_0, \boldsymbol{\Sigma}_0, a_0, b_0, \boldsymbol{\eta}_{\text{op}}, \boldsymbol{\eta}_{\text{ft}}, \alpha, \delta)$; optimized variational parameter vector: ϕ^* ; the operator set $\mathcal{O} = \mathcal{O}_u \cup \mathcal{O}_b$; the number of hard symbolic tree samples: H .

Output: A collection of H sampled hard symbolic ensembles and their corresponding posterior mean estimates of the model regression parameters: $\{\{\mathcal{T}(\mathfrak{E}_j^{(s)})\}_{j=1}^K, \boldsymbol{\beta}_{\text{PM}}^{(s)}, (\sigma^2)_{\text{PM}}^{(s)} : s = 1, \dots, H\}$.

for $s \leftarrow 1$ **to** H **do**

 // Sample one ensemble of K hard symbolic trees

for $j \leftarrow 1$ **to** K **do**

 // (i) sample expansion indicators

$\hat{e}_{j\zeta}^{(s)} \sim \text{Ber}(\sigma(\ell_{j\zeta}^*))$ for all $\zeta \in \mathcal{Z}_D$

 Enforce leaf constraint: $\hat{e}_{j\zeta}^{(s)} \leftarrow 0$ for all ζ at depth D

 // (ii) sample operator and feature labels

$\hat{o}_{j\zeta}^{(s)} \sim \text{Cat}(\text{softmax}((\mathbf{a}_{j\zeta}^{\text{op}})^*))$

$\hat{h}_{j\zeta}^{(s)} \sim \text{Cat}(\text{softmax}((\mathbf{a}_{j\zeta}^{\text{ft}})^*))$

 // (iii) Construct hard symbolic tree skeleton

$(\widehat{\mathcal{F}}_j^{(D)})^{(s)} \leftarrow \{\hat{e}_{j\zeta}^{(s)}, \hat{o}_{j\zeta}^{(s)}, \hat{h}_{j\zeta}^{(s)} : \zeta \in \mathcal{Z}_D\}$

 // (iv) symbolic trees via deterministic pruning of skeleton

$\mathcal{T}(\mathfrak{E}_j^{(s)}) \leftarrow \text{p}((\widehat{\mathcal{F}}_j^{(D)})^{(s)})$

for $i \leftarrow 1$ **to** n **do**

 // Evaluate at sample \mathbf{x}_i

$t_{ij}^{(s)} \leftarrow g(\mathbf{x}_i; \mathcal{T}(\mathfrak{E}_j^{(s)}))$

 // Construct expression design matrix

$t_{i0}^{(s)} \leftarrow 1$ for all $i = 1, \dots, n$

$\mathbf{T}^{(s)} \leftarrow ((t_{ij}^{(s)}))_{1 \leq i \leq n, 0 \leq j \leq K}$

 // Compute posterior means of model regression parameters

$\boldsymbol{\beta}_{\text{PM}}^{(s)} \leftarrow \mathbb{E}[\boldsymbol{\beta} \mid \sigma^2, \mathbf{T}^{(s)}, \mathbf{y}]$ and $(\sigma^2)_{\text{PM}}^{(s)} \leftarrow \mathbb{E}[\sigma^2 \mid \mathbf{T}^{(s)}, \mathbf{y}]$, using (G.2)

return $\{\{\mathcal{T}(\mathfrak{E}_j^{(s)})\}_{j=1}^K, \boldsymbol{\beta}_{\text{PM}}^{(s)}, (\sigma^2)_{\text{PM}}^{(s)} : s = 1, \dots, H\}$

G Technical Details

G.1 Marginalization of the Model Regression Parameters

The full joint posterior distribution as stated in (5) in Section 4 is:

$$\Pi(\Theta, \boldsymbol{\beta}, \sigma^2 \mid \mathcal{D}_n) \propto p(\mathbf{y} \mid \mathbf{T}, \boldsymbol{\beta}, \sigma^2) \Pi(\boldsymbol{\beta}, \sigma^2) \Pi(\mathbf{w}_{\text{op}}) \Pi(\mathbf{w}_{\text{ft}}) \prod_{j=1}^K \prod_{\zeta \in \mathcal{Z}_D} \Pi(e_{j\zeta}) \Pi(o_{j\zeta} \mid \mathbf{w}_{\text{op}}) \Pi(h_{j\zeta} \mid \mathbf{w}_{\text{ft}}). \quad (\text{G.1})$$

Under the Gaussian likelihood and the conjugate NIG prior:

$$\mathbf{y} \mid \boldsymbol{\beta}, \sigma^2, \mathbf{T} \sim N_n(\mathbf{T}\boldsymbol{\beta}, \sigma^2 \mathbf{I}_n), \quad \boldsymbol{\beta} \mid \sigma^2 \sim N_{K+1}(\boldsymbol{\mu}_0, \sigma^2 \boldsymbol{\Sigma}_0), \quad \sigma^2 \sim \text{IG}(a_0, b_0),$$

the posterior remains NIG:

$$\boldsymbol{\beta} \mid \sigma^2, \mathbf{T}, \mathbf{y} \sim N_{K+1}(\boldsymbol{\mu}_n, \sigma^2 \boldsymbol{\Sigma}_n), \quad \sigma^2 \mid \mathbf{T}, \mathbf{y} \sim \text{IG}(a_n, b_n), \quad (\text{G.2})$$

where the posterior hyperparameters are:

$$\boldsymbol{\Sigma}_n^{-1} = \boldsymbol{\Sigma}_0^{-1} + \mathbf{T}^\top \mathbf{T}, \quad \boldsymbol{\mu}_n = \boldsymbol{\Sigma}_n (\boldsymbol{\Sigma}_0^{-1} \boldsymbol{\mu}_0 + \mathbf{T}^\top \mathbf{y}), \quad a_n = a_0 + \frac{n}{2}, \quad b_n = b_0 + \frac{1}{2} \left(\mathbf{y}^\top \mathbf{y} + \boldsymbol{\mu}_0^\top \boldsymbol{\Sigma}_0^{-1} \boldsymbol{\mu}_0 - \boldsymbol{\mu}_n^\top \boldsymbol{\Sigma}_n^{-1} \boldsymbol{\mu}_n \right).$$

Integrating out $(\boldsymbol{\beta}, \sigma^2)$ yields the marginal likelihood:

$$\begin{aligned} p(\mathbf{y} \mid \mathbf{T}) &= \int p(\mathbf{y} \mid \mathbf{T}, \boldsymbol{\beta}, \sigma^2) \Pi(\boldsymbol{\beta}, \sigma^2) d\boldsymbol{\beta} d\sigma^2 \\ &= \frac{\Gamma(a_n)}{\Gamma(a_0)} \frac{|\boldsymbol{\Sigma}_n|^{\frac{1}{2}} b_0^{a_0}}{|\boldsymbol{\Sigma}_0|^{\frac{1}{2}} b_n^{a_n}} (2\pi)^{-\frac{n}{2}}, \end{aligned} \quad (\text{G.3})$$

where $\Gamma(\cdot)$ is the Gamma function as in Table A.1. Up to additive constants independent of \mathbf{T} , the log-marginal likelihood is therefore:

$$\log p(\mathbf{y} \mid \mathbf{T}) = \frac{1}{2} \log |\boldsymbol{\Sigma}_n| - a_n \log b_n + \log \Gamma(a_n) + C, \quad (\text{G.4})$$

where C collects terms independent of \mathbf{T} . Consequently, the marginal posterior over the tree parameters Θ becomes:

$$\Pi(\Theta \mid \mathcal{D}_n) \propto p(\mathbf{y} \mid \mathbf{T}) \Pi(\mathbf{w}_{\text{op}}) \Pi(\mathbf{w}_{\text{ft}}) \prod_{j=1}^K \prod_{\zeta \in \mathcal{Z}_D} \Pi(e_{j\zeta}) \Pi(o_{j\zeta} \mid \mathbf{w}_{\text{op}}) \Pi(h_{j\zeta} \mid \mathbf{w}_{\text{ft}}), \quad (\text{G.5})$$

which is the quantity of interest we approximate using an optimal variational family obtained by optimizing the variational objective.

G.2 Derivation of the Analytical Kullback–Leibler Divergence Terms

In this section, we provide a detailed derivation of the Kullback–Leibler (KL) term in (9) in Section 3.2. Specifically, this term corresponds to the KL divergence between the variational posterior $q_\phi(\Theta)$ in (8) and the prior $\Pi(\Theta)$ over the tree parameters in (4):

$$\begin{aligned} \text{KL}(q_\phi(\Theta) \parallel \Pi(\Theta)) &= \mathbb{E}_{q_\phi(\Theta)} \left[\log \frac{q_\phi(\Theta)}{\Pi(\Theta)} \right] \\ &= \mathbb{E}_{q_\phi(\Theta)} \left[\log \frac{q_\phi(\mathbf{w}_{\text{op}}) q_\phi(\mathbf{w}_{\text{ft}}) \prod_{j=1}^K \prod_{\zeta \in \mathcal{Z}_D} q_\phi(e_{j\zeta}) q_\phi(o_{j\zeta}) q_\phi(h_{j\zeta})}{\Pi(\mathbf{w}_{\text{op}}) \Pi(\mathbf{w}_{\text{ft}}) \prod_{j=1}^K \prod_{\zeta \in \mathcal{Z}_D} \Pi(e_{j\zeta}) \Pi(o_{j\zeta} \mid \mathbf{w}_{\text{op}}) \Pi(h_{j\zeta} \mid \mathbf{w}_{\text{ft}})} \right] \\ &= \mathbb{E}_{q_\phi(\Theta)} \left[\log \frac{q_\phi(\mathbf{w}_{\text{op}})}{\Pi(\mathbf{w}_{\text{op}})} + \log \frac{q_\phi(\mathbf{w}_{\text{ft}})}{\Pi(\mathbf{w}_{\text{ft}})} + \sum_{j=1}^K \sum_{\zeta \in \mathcal{Z}_D} \left(\log \frac{q_\phi(e_{j\zeta})}{\Pi(e_{j\zeta})} + \log \frac{q_\phi(o_{j\zeta})}{\Pi(o_{j\zeta} \mid \mathbf{w}_{\text{op}})} + \log \frac{q_\phi(h_{j\zeta})}{\Pi(h_{j\zeta} \mid \mathbf{w}_{\text{ft}})} \right) \right] \quad (\text{G.6}) \\ &= \text{KL}(q_\phi(\mathbf{w}_{\text{op}}) \parallel \Pi(\mathbf{w}_{\text{op}})) + \text{KL}(q_\phi(\mathbf{w}_{\text{ft}}) \parallel \Pi(\mathbf{w}_{\text{ft}})) + \sum_{j=1}^K \sum_{\zeta \in \mathcal{Z}_D} \left[\text{KL}(q_\phi(e_{j\zeta}) \parallel \Pi(e_{j\zeta})) \right. \\ &\quad \left. + \mathbb{E}_{q_\phi(\mathbf{w}_{\text{op}})} [\text{KL}(q_\phi(o_{j\zeta}) \parallel \Pi(o_{j\zeta} \mid \mathbf{w}_{\text{op}}))] + \mathbb{E}_{q_\phi(\mathbf{w}_{\text{ft}})} [\text{KL}(q_\phi(h_{j\zeta}) \parallel \Pi(h_{j\zeta} \mid \mathbf{w}_{\text{ft}}))] \right]. \end{aligned}$$

Now, we derive the analytic forms of each of the terms in the final sum in (G.6).

Lemma G.1 (KL divergence between Dirichlet distributions). *Let $q \equiv \text{Dir}(\tilde{\boldsymbol{\eta}})$ and $\pi \equiv \text{Dir}(\boldsymbol{\eta})$ on Δ^m , where $\tilde{\boldsymbol{\eta}}, \boldsymbol{\eta} \in (0, \infty)^m$. Define $\tilde{\eta}_0 = \sum_{k=1}^m \tilde{\eta}_k$. Then:*

$$\text{KL}(\text{Dir}(\tilde{\boldsymbol{\eta}}) \parallel \text{Dir}(\boldsymbol{\eta})) = \log \frac{\mathcal{B}(\boldsymbol{\eta})}{\mathcal{B}(\tilde{\boldsymbol{\eta}})} + \sum_{k=1}^m (\tilde{\eta}_k - \eta_k) [\Psi(\tilde{\eta}_k) - \Psi(\tilde{\eta}_0)], \quad (\text{G.7})$$

where $\mathcal{B}(\cdot)$ and $\Psi(\cdot)$ are the multivariate Beta and Digamma functions, respectively, as defined in Table A.1.

Proof. Let $\mathbf{w} \in \Delta^m$ such that $\mathbf{w} \sim q$. From the definition of KL divergence, we conclude:

$$\begin{aligned} \text{KL}(\text{Dir}(\tilde{\boldsymbol{\eta}}) \parallel \text{Dir}(\boldsymbol{\eta})) &= \mathbb{E}_q \left[\log \frac{q(\mathbf{w})}{\pi(\mathbf{w})} \right] = \mathbb{E}_q \left[\log \frac{\mathcal{B}(\boldsymbol{\eta})}{\mathcal{B}(\tilde{\boldsymbol{\eta}})} + \sum_{k=1}^m (\tilde{\eta}_k - \eta_k) \log w_k \right] \\ &= \log \frac{\mathcal{B}(\boldsymbol{\eta})}{\mathcal{B}(\tilde{\boldsymbol{\eta}})} + \sum_{k=1}^m (\tilde{\eta}_k - \eta_k) \mathbb{E}_q[\log w_k]. \end{aligned} \quad (\text{G.8})$$

It remains to compute $\mathbb{E}_q[\log w_k]$ under $q \equiv \text{Dir}(\tilde{\boldsymbol{\eta}})$. For any $k \in \{1, \dots, m\}$, using differentiation under the integral sign:

$$0 = \frac{\partial}{\partial \tilde{\eta}_k} \int_{\Delta^m} q(\mathbf{w}) d\mathbf{w} = \int_{\Delta^m} \frac{\partial}{\partial \tilde{\eta}_k} q(\mathbf{w}) d\mathbf{w}. \quad (\text{G.9})$$

Moreover:

$$\begin{aligned} \log q(\mathbf{w}) &= -\log \mathcal{B}(\tilde{\boldsymbol{\eta}}) + \sum_{r=1}^m (\tilde{\eta}_r - 1) \log w_r \\ \implies \frac{\partial}{\partial \tilde{\eta}_k} \log q(\mathbf{w}) &= -\frac{\partial}{\partial \tilde{\eta}_k} \log \mathcal{B}(\tilde{\boldsymbol{\eta}}) + \log w_k \\ \implies \frac{\partial}{\partial \tilde{\eta}_k} q(\mathbf{w}) &= q(\mathbf{w}) \left(-\frac{\partial}{\partial \tilde{\eta}_k} \log \mathcal{B}(\tilde{\boldsymbol{\eta}}) + \log w_k \right). \end{aligned} \quad (\text{G.10})$$

Substituting (G.10) into (G.9) and noting that $\int_{\Delta^m} q(\mathbf{w}) d\mathbf{w} = 1$ gives:

$$0 = -\frac{\partial}{\partial \tilde{\eta}_k} \log \mathcal{B}(\tilde{\boldsymbol{\eta}}) + \int_{\Delta^m} q(\mathbf{w}) \log w_k d\mathbf{w} = -\frac{\partial}{\partial \tilde{\eta}_k} \log \mathcal{B}(\tilde{\boldsymbol{\eta}}) + \mathbb{E}_q[\log w_k], \quad (\text{G.11})$$

and therefore:

$$\mathbb{E}_q[\log w_k] = \frac{\partial}{\partial \tilde{\eta}_k} \log \mathcal{B}(\tilde{\boldsymbol{\eta}}) = \frac{\partial}{\partial \tilde{\eta}_k} \left[\sum_{r=1}^m \log \Gamma(\tilde{\eta}_r) - \log \Gamma(\tilde{\eta}_0) \right] = \Psi(\tilde{\eta}_k) - \Psi(\tilde{\eta}_0). \quad (\text{G.12})$$

Substituting this expression into (G.8) gives (G.7), completing the proof. \square

Now, an application of Lemma G.1 yields the following:

$$\text{KL}(q_\phi(\mathbf{w}_{\text{op}}) \parallel \Pi(\mathbf{w}_{\text{op}})) = \log \frac{\mathcal{B}(\boldsymbol{\eta}_{\text{op}})}{\mathcal{B}(\tilde{\boldsymbol{\eta}}_{\text{op}})} + \sum_{k=1}^{|\mathcal{O}|} (\tilde{\eta}_{\text{op},k} - \eta_{\text{op},k}) \left(\Psi(\tilde{\eta}_{\text{op},k}) - \Psi(\mathbf{1}_{|\mathcal{O}|}^\top \tilde{\boldsymbol{\eta}}_{\text{op}}) \right), \quad (\text{G.13})$$

$$\text{KL}(q_\phi(\mathbf{w}_{\text{ft}}) \parallel \Pi(\mathbf{w}_{\text{ft}})) = \log \frac{\mathcal{B}(\boldsymbol{\eta}_{\text{ft}})}{\mathcal{B}(\tilde{\boldsymbol{\eta}}_{\text{ft}})} + \sum_{k=1}^p (\tilde{\eta}_{\text{ft},k} - \eta_{\text{ft},k}) \left(\Psi(\tilde{\eta}_{\text{ft},k}) - \Psi(\mathbf{1}_p^\top \tilde{\boldsymbol{\eta}}_{\text{ft}}) \right), \quad (\text{G.14})$$

where $\mathbf{1}_m$ is a m -dimensional vector of ones as in Table A.1. By definition, the KL divergence between two Bernoulli distributions $\text{Ber}(\tilde{p})$ and $\text{Ber}(p)$ is:

$$\text{KL}(\text{Ber}(\tilde{p}) \parallel \text{Ber}(p)) = \tilde{p} \log \frac{\tilde{p}}{p} + (1 - \tilde{p}) \log \frac{1 - \tilde{p}}{1 - p}. \quad (\text{G.15})$$

Consequently using (G.15):

$$\text{KL}(q_\phi(e_{j\zeta}) \parallel \Pi(e_{j\zeta})) = \tilde{p}_{j\zeta} \log \frac{\tilde{p}_{j\zeta}}{p_{j\zeta}} + (1 - \tilde{p}_{j\zeta}) \log \frac{1 - \tilde{p}_{j\zeta}}{1 - p_{j\zeta}}. \quad (\text{G.16})$$

Similarly, the KL divergence between two categorical distributions $\text{Cat}(\tilde{\boldsymbol{\pi}})$ and $\text{Cat}(\mathbf{w})$ is:

$$\text{KL}(\text{Cat}(\tilde{\boldsymbol{\pi}}) \parallel \text{Cat}(\mathbf{w})) = \sum_{k=1}^m \tilde{\pi}_k \log \frac{\tilde{\pi}_k}{w_k} = \sum_{k=1}^m \tilde{\pi}_k [\log \tilde{\pi}_k - \log w_k], \quad (\text{G.17})$$

which implies:

$$\begin{aligned} \mathbb{E}_{q_\phi(\mathbf{w}_{\text{op}})} [\text{KL}(q_\phi(o_{j\zeta}) \parallel \Pi(o_{j\zeta} \mid \mathbf{w}_{\text{op}}))] &= \sum_{k=1}^{|\mathcal{O}|} \tilde{\pi}_{j\zeta,k}^{\text{op}} \left[\log(\tilde{\pi}_{j\zeta,k}^{\text{op}}) - \mathbb{E}_{q_\phi(\mathbf{w}_{\text{op}})}[\log w_k] \right] \\ &= \sum_{k=1}^{|\mathcal{O}|} \tilde{\pi}_{j\zeta,k}^{\text{op}} \left[\log(\tilde{\pi}_{j\zeta,k}^{\text{op}}) - \Psi(\tilde{\boldsymbol{\eta}}_{\text{op},k}) + \Psi(\mathbf{1}_{|\mathcal{O}|}^\top \tilde{\boldsymbol{\eta}}_{\text{op}}) \right], \end{aligned} \quad (\text{G.18})$$

where the last equality follows from (G.12) in the proof of Lemma G.1. Analogously:

$$\mathbb{E}_{q_\phi(\mathbf{w}_{\text{ft}})} [\text{KL}(q_\phi(h_{j\zeta}) \parallel \Pi(h_{j\zeta} \mid \mathbf{w}_{\text{ft}}))] = \sum_{k=1}^p \tilde{\pi}_{j\zeta,k}^{\text{ft}} \left[\log(\tilde{\pi}_{j\zeta,k}^{\text{ft}}) - \Psi(\tilde{\boldsymbol{\eta}}_{\text{ft},k}) + \Psi(\mathbf{1}_p^\top \tilde{\boldsymbol{\eta}}_{\text{ft}}) \right]. \quad (\text{G.19})$$

Putting together (G.13), (G.14), (G.16), (G.18), and (G.19) in (G.6), we get the following composite expression for the KL component:

$$\begin{aligned} \text{KL}(q_\phi(\Theta) \parallel \Pi(\Theta)) &= \log \frac{\mathcal{B}(\boldsymbol{\eta}_{\text{op}})}{\mathcal{B}(\tilde{\boldsymbol{\eta}}_{\text{op}})} + \sum_{k=1}^{|\mathcal{O}|} (\tilde{\boldsymbol{\eta}}_{\text{op},k} - \boldsymbol{\eta}_{\text{op},k}) \left(\Psi(\tilde{\boldsymbol{\eta}}_{\text{op},k}) - \Psi(\mathbf{1}_{|\mathcal{O}|}^\top \tilde{\boldsymbol{\eta}}_{\text{op}}) \right) + \log \frac{\mathcal{B}(\boldsymbol{\eta}_{\text{ft}})}{\mathcal{B}(\tilde{\boldsymbol{\eta}}_{\text{ft}})} \\ &+ \sum_{k=1}^p (\tilde{\boldsymbol{\eta}}_{\text{ft},k} - \boldsymbol{\eta}_{\text{ft},k}) \left(\Psi(\tilde{\boldsymbol{\eta}}_{\text{ft},k}) - \Psi(\mathbf{1}_p^\top \tilde{\boldsymbol{\eta}}_{\text{ft}}) \right) + \sum_{j=1}^K \sum_{\zeta \in \mathcal{Z}_D} \left[\tilde{p}_{j\zeta} \log \frac{\tilde{p}_{j\zeta}}{p_\zeta} + (1 - \tilde{p}_{j\zeta}) \log \frac{1 - \tilde{p}_{j\zeta}}{1 - p_\zeta} \right] \\ &+ \sum_{k=1}^{|\mathcal{O}|} \tilde{\pi}_{j\zeta,k}^{\text{op}} \left[\log(\tilde{\pi}_{j\zeta,k}^{\text{op}}) - \Psi(\tilde{\boldsymbol{\eta}}_{\text{op},k}) + \Psi(\mathbf{1}_{|\mathcal{O}|}^\top \tilde{\boldsymbol{\eta}}_{\text{op}}) \right] + \sum_{k=1}^p \tilde{\pi}_{j\zeta,k}^{\text{ft}} \left[\log(\tilde{\pi}_{j\zeta,k}^{\text{ft}}) - \Psi(\tilde{\boldsymbol{\eta}}_{\text{ft},k}) + \Psi(\mathbf{1}_p^\top \tilde{\boldsymbol{\eta}}_{\text{ft}}) \right]. \end{aligned} \quad (\text{G.20})$$

H Configurations of VaSST and Competing Methods

H.1 Experimental Settings of VaSST

Here we outline the experimental configuration of VaSST used for learning the symbolic expressions in Section 5.1 and the Feynman equations in Section 5.2.

For both the simulation experiments in Section 5.1 and the Feynman equations in Section 5.2, we employ the operator set $\mathcal{O} = \{+, \times, -, /, \exp, \log, \sin, \cos, ^2\}$, and fix the number of symbolic trees to $K = 3$ and the maximum depth per tree to $D = 3$. This configuration provides adequate representational capacity in learning the symbolic structures considered in Sections 5.1 and 5.2. The depth-adaptive split probability prior in (3) is governed by $(\alpha, \delta) = (0.95, 2.00)$, which effectively penalizes overly complex output expressions and promotes structural parsimony. The prior hyperparameters over the model regression parameters $(\boldsymbol{\beta}, \boldsymbol{\sigma}^2)$ in Section 3.1 are configured as: $(\boldsymbol{\mu}_0, \boldsymbol{\Sigma}_0, a_0, b_0) = (\mathbf{0}_{K+1}, 10\mathbf{I}_{K+1}, 2, 2)$ along with the operator and feature assignments in (3) following uniform Dirichlet priors, i.e., $\boldsymbol{\eta}_{\text{op}} = \mathbf{1}_{|\mathcal{O}|}$ and $\boldsymbol{\eta}_{\text{ft}} = \mathbf{1}_p$.

Variational optimization is performed using AdamW [Loshchilov and Hutter, 2019] (having a learning rate of $\gamma = 5 \times 10^{-5}$, optimizer hyperparameters set as $(0.90, 0.99)$, and no weight decay) for 2000 iterations (or steps), with $S = 8$ Monte Carlo samples per ELBO step and gradient clipping at $c = 1.0$. The Binary Concrete and Gumbel-Softmax temperatures in (12) are annealed linearly from $\tau_{\text{start}} = 1.0$ to $\tau_{\text{end}} = 0.5$ over $T_\tau = 1500$ steps. After training on the 90% train split, $H = 2000$ hard symbolic tree ensembles are sampled from the learned variational distribution. For each sampled structure, the posterior mean estimates of $(\boldsymbol{\beta}, \boldsymbol{\sigma}^2)$ are computed, and symbolic expressions are ranked according to minimum in-sample RMSE evaluated.

H.2 Experimental Settings of QLattice

QLattice [Broløs et al., 2021] is implemented via the Feyn Python interface², a supervised machine learning framework designed to perform symbolic regression. We use the default configuration of QLattice across all applications in Sections 5.1 and 5.2, with the number of training epochs set to 25.

The operator set, referred to as *interactions* in the QLattice–Feyn interface, is configured as \mathcal{O} in Section H.1, ensuring consistency with the operator set used for VaSST. Predictive performance is assessed using out-of-sample RMSE computed on the 10% held-out test set, following the same evaluation protocol adopted for VaSST.

H.3 Experimental Settings of gplearn and DEAP

gplearn. We employ the gplearn [Stephens, 2016] symbolic regression framework³ implemented in Python and outline its experimental configuration for learning the symbolic expressions in Section 5.1 and the Feynman equations in Section 5.2. The SymbolicRegressor is configured with a population size of 2000 and evolved for 20 generations using tournament selection with tournament size 20. The function set is restricted to \mathcal{O} as in Section H.1 to match that of VaSST. The fitness metric is set to RMSE, and a parsimony coefficient of 10^{-4} is used to penalize overly complex expressions. Predictive performance is evaluated as in VaSST, i.e., using out-of-sample RMSE on the 10% held-out test split.

Distributed Evolutionary algorithms in Python (DEAP). We implement genetic programming for symbolic regression using the DEAP⁴ [Fortin et al., 2012] framework, a general-purpose evolutionary computation library in Python. The experimental configurations of DEAP used in Sections 5.1 and 5.2 are as follows. Symbolic expressions are evolved using a $(\mu + \lambda)$ evolutionary strategy with $\mu = 200$ parent individuals and $\lambda = 200$ offspring per generation, for 20 generations. The crossover and mutation probabilities are set to 0.5 and 0.2, respectively. The primitive set includes binary and unary operators as in \mathcal{O} specified in Section H.1, along with ephemeral random constants sampled from $\text{Unif}(-5, 5)$. Fitness is measured using RMSE, and the best individual is selected from the *Hall-of-Fame archive* after evolution. Predictive accuracy is evaluated using out-of-sample RMSE on the 10% held-out test set.

H.4 Experimental Settings of BMS and BSR

Bayesian Machine Scientist (BMS). For BMS [Guimerà et al., 2020], we use the AutoRA implementation⁵ with default prior specifications and restrict the symbolic grammar to match the operator set \mathcal{O} used in VaSST in Section H.1 for

²Feyn–Symbolic AI using QLattice: <https://docs.abzu.ai/>

³gplearn Github repository: <https://github.com/trevorstephens/gplearn>

⁴DEAP Github repository: <https://github.com/DEAP/deap>

⁵AutoRA BMS implementation: <https://github.com/AutoResearch/autora-theorist-bms>

both the simulation study (Section 5.1) and the Feynman equations (Section 5.2). Model discovery is carried out via MCMC over the symbolic grammar space, with training conducted for 2000 epochs. All experiments are performed using the same 90/10 train–test split as VaSST, and predictive performance is assessed using out-of-sample RMSE computed on the held-out 10% test set.

Bayesian Symbolic Regression (BSR). For BSR [Jin et al., 2020], we employ the AutoRA implementation⁶ with the number of trees aligned to the ensemble size used in VaSST in Section H.1 across both the simulation experiments (Section 5.1) and the Feynman equations (Section 5.2). The number of MCMC iterations is set to 2000, and the operator set is restricted to \mathcal{O} , as in VaSST in Section H.1, to ensure consistency. Default prior hyperparameters are retained. Structure proposals are generated through stochastic tree operations within the MCMC procedure. To ensure fairness in comparison, the split probability configuration for node expansion is matched to that used in VaSST, as specified in (3) with corresponding hyperparameters (α, δ) in Section H.1. After convergence, regression coefficients are estimated using ordinary least squares, and predictive accuracy is evaluated using out-of-sample RMSE on the held-out 10% test split.

⁶AutoRA BSR implementation: <https://github.com/AutoResearch/autora-theorist-bsr>

I Additional Results for Simulation Experiments

I.1 Symbolic Expressions Learned by VaSST and Competing Methods

$$\text{For } \mathbf{y} = \mathbf{x}_0^2 - \mathbf{x}_1 + \frac{1}{2}\mathbf{x}_2^2.$$

Table I.1: Symbolic expressions recovered by VaSST ($K = 3$ and $D = 3$) and competing methods in a single run when learning (15) under noiseless setting. For `gplearn`: $A = \mathbf{x}_0^2 + \frac{\mathbf{x}_2}{\mathbf{x}_1} + 4\mathbf{x}_2 - \mathbf{x}_0 - 1.286$, $C = \frac{\mathbf{x}_1 - \mathbf{x}_2}{A}$, and $B = 1.843 + C + 0.373\mathbf{x}_2^2 - 0.08952\mathbf{x}_2$.

Method	Symbolic Expression Learned
VaSST	$0.003649 + 1.000895(\mathbf{x}_0^2 - \mathbf{x}_1) + 0.533075\mathbf{x}_2^2 + 0.007762\mathbf{x}_2$
BMS	$\left(a_0 + \frac{\sin(a_0)}{\mathbf{x}_1 + \mathbf{x}_2}\right)\mathbf{x}_2^{\sqrt{a_0}} + \mathbf{x}_0$; a_0 is a constant learned by BMS
BSR	$17.26 - 1.94 \ln(\mathbf{x}_1) + 0.07\left(\mathbf{x}_1 - \mathbf{x}_0\mathbf{x}_2 + \frac{1}{\cos(\mathbf{x}_2)}\right) + 0.02 e^{\mathbf{x}_1} \mathbf{x}_1$
QLattice	$-1.24(-0.26\mathbf{x}_0 - 0.22)(3.14\mathbf{x}_0 - 2.65) - 1.24(0.07\mathbf{x}_2 + 0.42)(0.98\mathbf{x}_1 - 5.20\mathbf{x}_2 + 24.17) + 11.30$
gplearn	$\frac{\mathbf{x}_1 - \mathbf{x}_2}{(0.382\mathbf{x}_2 - 1)B} + 0.373\mathbf{x}_2^2 + \mathbf{x}_2 + \mathbf{x}_0 - \mathbf{x}_1 - 1 \frac{\mathbf{x}_0 - \mathbf{x}_2 - \mathbf{x}_0\mathbf{x}_2}{(\mathbf{x}_0^3 + 0.382\mathbf{x}_2 - 1)(\mathbf{x}_1 - 0.438 - 0.382\mathbf{x}_2^2)}$
DEAP	$1.17((\mathbf{x}_0 + 1.41^2) \times (\mathbf{x}_2 - 4.78)) + 2\mathbf{x}_2$

Table I.2: Symbolic expressions recovered by VaSST ($K = 3$ and $D = 3$) and competing methods in a single run when learning (15) under an added noise level of $\sigma^2 = 0.2^2$.

Method	Symbolic Expression Learned
VaSST	$-0.007736 + 0.537259(\mathbf{x}_0^2 + \mathbf{x}_0^2) - 1.037259\mathbf{x}_1 + 0.512466\mathbf{x}_2^2$
BMS	$a_0^2\mathbf{x}_2^2 - \mathbf{x}_1 + \mathbf{x}_0$; a_0 is a constant learned by BMS
BSR	$-3.05 + 0.03 \cos((\mathbf{x}_0 - \ln(\mathbf{x}_2))^2) + 0.50\mathbf{x}_2^2 + 0.59 \exp(\mathbf{x}_0^2)$
QLattice	$-5.46(1.68 - 0.00103\mathbf{x}_0)\left(0.113\mathbf{x}_1 - \tanh(0.620\mathbf{x}_2 - 3.55) - 1.74 + \exp(-0.122(\mathbf{x}_0 - 0.0565)^2)\right) + 9.70$
gplearn	$\left(\frac{\mathbf{x}_1 - \mathbf{x}_2}{(0.382\mathbf{x}_2 - 1)\left(1.843 + \frac{\mathbf{x}_1 - \mathbf{x}_2}{\mathbf{x}_0^2 + \frac{\mathbf{x}_2}{\mathbf{x}_1} + 4\mathbf{x}_2 - \mathbf{x}_0 - 1.286} + 0.373\mathbf{x}_2^2 - 0.0895\mathbf{x}_2\right)} + 0.373\mathbf{x}_2^2 + \mathbf{x}_2 + \mathbf{x}_0 - \mathbf{x}_1 - 1 - \frac{\mathbf{x}_0 - \mathbf{x}_2 - \mathbf{x}_0\mathbf{x}_2}{(\mathbf{x}_0^3 + 0.382\mathbf{x}_2 - 1)(\mathbf{x}_1 - 0.438 - 0.382\mathbf{x}_2^2)}\right)$
DEAP	$1.17((\mathbf{x}_0 + 1.41^2) \times (\mathbf{x}_2 - 4.78)) + 2\mathbf{x}_2$

$$\text{For } \mathbf{y} = 6 \sin(\mathbf{x}_0) \cos(\mathbf{x}_1).$$

Table I.3: Symbolic expressions recovered by VaSST ($K = 3$ and $D = 3$) and competing methods in a single run when learning (16) under noiseless setting.

Method	Symbolic Expression Learned
VaSST	$-0.004604 + 0.001381 \sin(\mathbf{x}_1) + 0.001381 \sin(\mathbf{x}_1) + 5.992116 \sin(\mathbf{x}_0) \cos(\mathbf{x}_1)$
BMS	$a_0 \sin(\mathbf{x}_0) \cos(\mathbf{x}_1)$; a_0 is a constat learned by BMS
BSR	$4.62 - 3.83(\mathbf{x}_1 - \mathbf{x}_0) + 0.758 \mathbf{x}_1^2 - 3.10(\mathbf{x}_0 \mathbf{x}_1)$
QLattice	$2.7271(-2.21173 \mathbf{x}_0 - 7.6632 \times 10^{-5}) \exp(-0.183142(\mathbf{x}_0 - 0.0397885)^2 - 0.908395(-0.0990112 \mathbf{x}_1 - 1)^2 \log(0.457843 \mathbf{x}_1 - 0.4763)^2) - 2.64677 \times 10^{-4}$
gplearn	$-\frac{\mathbf{x}_0}{0.413 \mathbf{x}_1} (\mathbf{x}_1^2 - \mathbf{x}_0 - 1.194)$
DEAP	$-1.72 \mathbf{x}_0 \mathbf{x}_1$

Table I.4: Symbolic expressions recovered by VaSST ($K = 3$ and $D = 3$) and competing methods in a single run when learning (16) under an added noise level of $\sigma^2 = 0.1^2$.

Method	Symbolic Expression Learned
VaSST	$0.007364 - 0.001479 \cos(\cos(\cos(\mathbf{x}_0))) + 0.005776 \sin(\cos(\mathbf{x}_0)) \cos(\mathbf{x}_0) + 5.990218 \sin(\mathbf{x}_0) \cos(\mathbf{x}_1)$
BMS	$a_0 \sin(\mathbf{x}_0) \cos(\mathbf{x}_1)$; a_0 is a constant learned by BMS
BSR	$-7.9825 + 9.51062 \exp((\ln(\mathbf{x}_1))(\mathbf{x}_0)) - 1.32812 \cos(-\sin(\mathbf{x}_0))$
QLattice	$-2.7354(1.86589 \tanh(1.30367 \mathbf{x}_1 - 2.60134) + 1.13614) \tanh(0.805853 \mathbf{x}_0 - 0.000700283) - 0.00773843$
gplearn	$-\frac{\mathbf{x}_0}{0.413 \mathbf{x}_1} (\mathbf{x}_1^2 - \mathbf{x}_0 - 1.223)$
DEAP	$-1.722 \mathbf{x}_0 \mathbf{x}_1$

Table I.5: Symbolic expressions recovered by VaSST ($K = 3$ and $D = 3$) and competing methods in a single run when learning (16) under an added noise level of $\sigma^2 = 0.2^2$.

Method	Symbolic Expression Learned
VaSST	$0.001577 - 0.002600 \cos(\cos(\cos(\mathbf{x}_0))) + 0.007118 \sin(\cos(\mathbf{x}_0)) \cos(\mathbf{x}_0) + 6.009543 \sin(\mathbf{x}_0) \cos(\mathbf{x}_1)$
BMS	$a_0 \sin(\mathbf{x}_0) \cos(\mathbf{x}_1)$; a_0 is a constant learned by BMS
BSR	$-7.96754 + 9.54025 \exp((\ln(\mathbf{x}_1))(\mathbf{x}_0)) - 1.37319 \cos(-\sin(\mathbf{x}_0))$
QLattice	$2.80929(-2.11692 \mathbf{x}_0 - 0.0220998) \exp(-0.348625(0.348892 - \mathbf{x}_0)^2 - 16.9016(0.260553 \mathbf{x}_1 - 1)^4) + 0.0240098$
gplearn	$-\frac{\mathbf{x}_0}{0.413(\mathbf{x}_1 + 0.222)} (\mathbf{x}_1^2 - \mathbf{x}_0 - 0.873)$
DEAP	$-1.722 \mathbf{x}_0 \mathbf{x}_1$

I.2 Out-of-sample RMSE for VaSST and competing methods

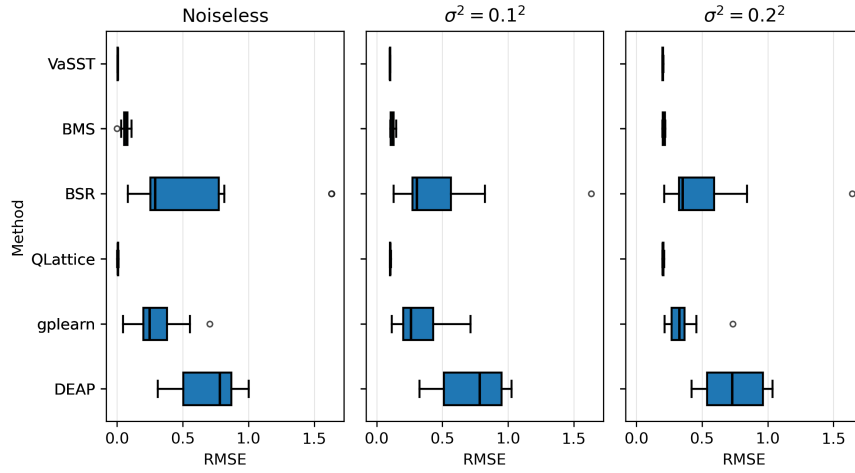


Figure I.1: Out-of-sample RMSEs over 10 repetitions of a 90/10 train-test split for VaSST ($K = 3$ and $D = 3$) and competing methods across varying noise settings while learning $\mathbf{y} = \mathbf{x}_0^2 - \mathbf{x}_1 + \frac{1}{2}\mathbf{x}_2^2$ in (15).

Table I.6: Out-of-sample RMSEs (computed on a 10% held-out test set) of VaSST ($K = 3$ and $D = 3$) and competing methods over 10 repetitions (mean \pm standard deviation) for learning $\mathbf{y} = 6 \sin(\mathbf{x}_0) \cos(\mathbf{x}_1)$ in (16) across all noise settings.

Noiseless		$\sigma^2 = 0.1^2$		$\sigma^2 = 0.2^2$	
Method	Mean \pm Std. Dev.	Method	Mean \pm Std. Dev.	Method	Mean \pm Std. Dev.
VaSST	0.001679 \pm 0.000378	VaSST	0.099378 \pm 0.000920	VaSST	0.198707 \pm 0.001831
BMS	0.002887 \pm 0.002660	QLattice	0.100077 \pm 0.000949	BMS	0.199005 \pm 0.001849
QLattice	0.003378 \pm 0.001521	BMS	0.103367 \pm 0.011609	QLattice	0.200107 \pm 0.002078
gplearn	0.101421 \pm 0.020990	gplearn	0.142202 \pm 0.014773	gplearn	0.225375 \pm 0.010239
DEAP	0.231622 \pm 0.126678	DEAP	0.248676 \pm 0.123758	DEAP	0.311183 \pm 0.106561
BSR	0.418971 \pm 0.290144	BSR	0.436781 \pm 0.281088	BSR	0.478658 \pm 0.264501

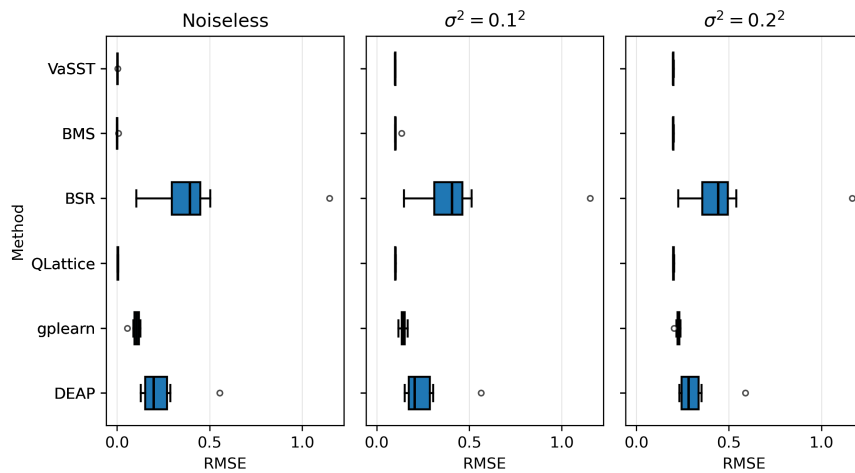


Figure I.2: Out-of-sample RMSEs over 10 repetitions of a 90/10 train-test split for VaSST ($K = 3$ and $D = 3$) and competing methods across varying noise settings while learning $\mathbf{y} = 6 \sin(\mathbf{x}_0) \cos(\mathbf{x}_1)$ in (16).

I.3 Top Symbolic Expressions Learned by VaSST

$$\text{For } \mathbf{y} = \mathbf{x}_0^2 - \mathbf{x}_1 + \frac{1}{2}\mathbf{x}_2^2.$$

Table I.7: Top 5 ranked symbolic expressions recovered by VaSST ($K = 3$ and $D = 3$) for a single run under the noiseless setting. Expressions are ranked by minimum in-sample RMSE among $H = 2000$ sampled hard symbolic trees.

Rank	Symbolic Expression
1	$-0.00240249 + 0.999157\mathbf{x}_0^2 - 1.00014\mathbf{x}_1 + 0.512214\mathbf{x}_2^2$
2	$-0.00247674 - 1.000159\mathbf{x}_1 - 0.999152\mathbf{x}_0^2 - 0.51272\mathbf{x}_2^2$
3	$-0.00245781 - 0.00168\mathbf{x}_1 + 0.51272\mathbf{x}_2^2 - 0.999292(\mathbf{x}_1 - \mathbf{x}_0^2)$
4	$-0.00302627 + 0.517348\mathbf{x}_2^2 - 0.998458\mathbf{x}_1 + 0.998458\mathbf{x}_0^2$
5	$0.002406054 + 0.998763\mathbf{x}_0^2 - 0.991904\mathbf{x}_1 + 0.604618\mathbf{x}_2^2$

Table I.8: Top 5 ranked symbolic expressions recovered by VaSST ($K = 3$ and $D = 3$) for a single run under noise level $\sigma^2 = 0.1^2$. Expressions are ranked by minimum in-sample RMSE among $H = 2000$ sampled hard symbolic trees.

Rank	Symbolic Expression
1	$0.002462065 + -1.000598\mathbf{x}_1 + 0.990598\mathbf{x}_0^2 + 0.606405\mathbf{x}_2^2$
2	$0.002475559 + 0.990459\mathbf{x}_0^2 - 1.00633\mathbf{x}_1 + 0.606124\mathbf{x}_2^2$
3	$0.0016037 + 1.001789\mathbf{x}_0^2 - 1.001789\mathbf{x}_1 + 0.524304\mathbf{x}_2^2$
4	$-0.00775405 + 1.00917\mathbf{x}_0^2 - 1.00917\mathbf{x}_1 + 0.512341\mathbf{x}_2^2$
5	$0.001851381 + 0.992129\mathbf{x}_0^2 - 1.202066\mathbf{x}_1 + 0.635361\mathbf{x}_2^2$

Table I.9: Top 5 ranked symbolic expressions recovered by VaSST ($K = 3$ and $D = 3$) for a single run under noise level $\sigma^2 = 0.2^2$. Expressions are ranked by minimum in-sample RMSE among $H = 2000$ sampled hard symbolic trees.

Rank	Symbolic Expression
1	$-0.000532 + 1.00432\mathbf{x}_0^2 - 1.00432\mathbf{x}_1 + 0.524445\mathbf{x}_2^2$
2	$0.001866003 + 0.983853\mathbf{x}_0^2 - 1.20505\mathbf{x}_1 + 0.635559\mathbf{x}_2^2$
3	$0.00121585 + 0.489214(\mathbf{x}_0^2 + \mathbf{x}_0^2) - 1.00486\mathbf{x}_1 + 0.583266\mathbf{x}_2^2$
4	$0.002607317 + 1.015483\mathbf{x}_0^2 - 1.015483\mathbf{x}_1 + 0.610346\mathbf{x}_2^2 - 0.001047438(\mathbf{x}_0 + \mathbf{x}_2)$
5	$-0.00887898 + 0.983157\mathbf{x}_0^2 - 1.206414\mathbf{x}_1 + 0.531632\mathbf{x}_2^2$

For $\mathbf{y} = 6 \sin(\mathbf{x}_0) \cos(\mathbf{x}_1)$.

Table I.10: Top 5 ranked symbolic expressions recovered by VaSST ($K = 3$ and $D = 3$) for a single run under the noiseless setting. Expressions are ranked by minimum in-sample RMSE among $H = 2000$ sampled hard symbolic trees.

Rank	Symbolic Expression
1	$-0.004604 + 0.001381 \sin(\mathbf{x}_1) + 0.001381 \sin(\mathbf{x}_1) + 5.992116 \sin(\mathbf{x}_0) \cos(\mathbf{x}_1)$
2	$0.085483 - 0.00162434 \cos(\cos(\mathbf{x}_0)) \cos(\sin(\mathbf{x}_0)) + 0.000628 \sin(\sin(\mathbf{x}_1) \sin(\mathbf{x}_0)) + 5.984428 \sin(\mathbf{x}_0) \cos(\mathbf{x}_1)$
3	$-0.0050173 - 0.000305 \cos(\mathbf{x}_1^2) + 0.0061529 \sin(\sin(\cos(\mathbf{x}_0))) + 5.975079 \sin(\mathbf{x}_0) \cos(\mathbf{x}_1)$
4	$-0.0045536 + 0.0039723 \cos(\sin(\mathbf{x}_0)) + 5.961262 \sin(\mathbf{x}_0) \cos(\mathbf{x}_1) - 0.0001790 \mathbf{x}_1^2 \mathbf{x}_0^3$
5	$-0.0049888 + 0.0081351 \cos(\mathbf{x}_0) - 0.0016211 \mathbf{x}_1 + 5.938406 \sin(\mathbf{x}_0) \cos(\mathbf{x}_1)$

Table I.11: Top 5 ranked symbolic expressions recovered by VaSST ($K = 3$ and $D = 3$) for a single run under noise level $\sigma^2 = 0.1^2$. Expressions are ranked by the minimum in-sample RMSE among $H = 2000$ sampled hard symbolic trees.

Rank	Symbolic Expression
1	$0.00180541 - 0.00344171 \cos(\cos(\mathbf{x}_0)) \cos(\sin(\mathbf{x}_0)) + 0.001757 \sin(\sin(\mathbf{x}_1) \sin(\mathbf{x}_0)) + 5.973780 \sin(\mathbf{x}_0) \cos(\mathbf{x}_1)$
2	$-0.005632 + -0.000336 \sin(\mathbf{x}_1) + -0.000336 \sin(\mathbf{x}_1) + 5.992481 \sin(\mathbf{x}_0) \cos(\mathbf{x}_1)$
3	$-0.0015351 + -0.001300 \cos(\mathbf{x}_1^2) + 0.0012336 \sin(\sin(\cos(\mathbf{x}_0))) + 5.988531 \sin(\mathbf{x}_0) \cos(\mathbf{x}_1)$
4	$-0.0087869 + 0.0083538 \cos(\sin(\mathbf{x}_0)) + 5.980441 \sin(\mathbf{x}_0) \cos(\mathbf{x}_1) + 0.003126 \mathbf{x}_1^2 \mathbf{x}_0^3$
5	$-0.0029653 + 0.0035745 \cos(\mathbf{x}_0) - 0.005924 \mathbf{x}_1 + 5.968753 \sin(\mathbf{x}_0) \cos(\mathbf{x}_1)$

Table I.12: Top 5 ranked symbolic expressions recovered by VaSST ($K = 3$ and $D = 3$) for a single run under noise level $\sigma^2 = 0.2^2$. Expressions are ranked by the minimum in-sample RMSE among $H = 2000$ sampled hard symbolic trees.

Rank	Symbolic Expression
1	$-0.00130203 + 0.00127353 \cos(\sin(\mathbf{x}_0)) + 5.999621 \sin(\mathbf{x}_0) \cos(\mathbf{x}_1) + 0.008042 \mathbf{x}_1^2 \mathbf{x}_0^3$
2	$0.0019471 - 0.002296 \cos(\mathbf{x}_1^2) - 0.0036858 \sin(\sin(\cos(\mathbf{x}_0))) + 6.001983 \sin(\mathbf{x}_0) \cos(\mathbf{x}_1)$
3	$0.00275600 + -0.00525907 \cos(\cos(\mathbf{x}_0)) \cos(\sin(\mathbf{x}_0)) + 0.002886 \sin(\sin(\mathbf{x}_1) \sin(\mathbf{x}_0)) + 5.963133 \sin(\mathbf{x}_0) \cos(\mathbf{x}_1)$
4	$0.000288 + 5.882739 \sin(\sin(\mathbf{x}_0)) \cos(\mathbf{x}_1) + -0.0073618 \mathbf{x}_0^2 \mathbf{x}_1^2 + -0.0048759 \mathbf{x}_0$
5	$-0.009418 - 0.009862 \cos(\mathbf{x}_0) + 0.004362 \mathbf{x}_1 + 5.999100 \sin(\mathbf{x}_0) \cos(\mathbf{x}_1)$

J Details on Feynman Equations

Table J.1: Response variables and input features for the Feynman equations in Section 5.2.

Feynman equation	Variable	Type	Description
CL: $F = 0.08 \frac{q_1 q_2}{\epsilon r^2}$	F	Response	Electrostatic force between two charges
	q_1, q_2	Input	Charge of two particles
	r	Input	Distance between the two charges
	ϵ	Constant	Permittivity of the medium
CPE: $\Delta U = G m_1 m_2 \left(\frac{1}{r_2} - \frac{1}{r_1} \right)$	ΔU	Response	Change in gravitational potential energy
	m_1, m_2	Input	Mass of two objects
	r_1, r_2	Input	Initial and final separation distances
	G	Constant	Gravitational constant
FCE: $F = q(E_f + vB \sin \theta)$	F	Response	Force on a moving charge in an EM field
	q	Input	Electric charge of the particle
	E_f	Input	Electric field strength
	v	Input	Particle velocity magnitude
	B	Input	Magnetic field strength
	θ	Input	Angle between velocity and magnetic field
FTC: $P = \frac{\kappa A (T_2 - T_1)}{d}$	P	Response	Rate of heat transfer (thermal power)
	A	Input	Cross-sectional area for heat flow
	T_1, T_2	Input	Temperature at first and second boundaries
	d	Input	Distance between the two temperature points
	κ	Constant	Thermal conductivity of material

K Additional Results for Feynman Equations

K.1 Expression Learned by VaSST and Competing Methods

K.1.1 Learning CL

Table K.1: Symbolic expressions recovered by VaSST ($K = 3$ and $D = 3$) and competing methods for **CL:** $F = 0.08 \epsilon^{-1} q_1 q_2 r^{-2}$ under the noiseless setting. Out-of-sample RMSE is evaluated on a 10% held-out test set, with all coefficients in the symbolic expression reported up to three decimal places across all methods.

Method	Symbolic Expression Learned	RMSE
VaSST	$0.080 \epsilon^{-1} q_1 q_2 r^{-2}$	4.67×10^{-5}
BMS	$0.080 \epsilon^{-1} q_1 q_2 r^{-2}$	0.0
BSR	$-1.305 + 0.579 \ln \left(\epsilon^{-1} q_1^2 r^{-2} \right) - 0.307 \sin \left(\cos \left(\frac{q_2}{q_1} \right) \right)$	2.29×10^{-2}
QLattice	$0.080 \epsilon^{-1} q_1 q_2 r^{-2}$	4.27×10^{-6}
gplearn	$0.081 \epsilon^{-1} q_1 q_2 r^{-2}$	5.71×10^{-3}
DEAP	$0.209 \epsilon^{-1} q_1^2 r^{-2}$	4.51×10^{-2}

Table K.2: Symbolic expressions recovered by VaSST ($K = 3$ and $D = 3$) and competing methods for **CL**: $F = 0.08\epsilon^{-1}q_1q_2r^{-2}$ under $\sigma^2 = 0.1^2$. Out-of-sample RMSE is evaluated on a 10% held-out test set, with all coefficients in the symbolic expression reported up to three decimal places across all methods.

Method	Symbolic Expression Learned	RMSE
VaSST	$-0.008 + 0.088\epsilon^{-1}q_1q_2r^{-2}$	1.00314×10^{-1}
BMS	$0.079\epsilon^{-1}q_1q_2r^{-2}$	1.00488×10^{-1}
BSR	$-1.250 + 0.559 \ln\left(\epsilon^{-1}q_1^2r^{-2}\right) - 0.291 \sin\left(\cos\left(\frac{q_2}{q_1}\right)\right)$	1.02342×10^{-1}
QLattice	$0.073\epsilon^{-1}q_1q_2r^{-2} - 0.004$	1.00534×10^{-1}
gplearn	$0.077\epsilon^{-1}q_1q_2r^{-2}$	1.00826×10^{-1}
DEAP	$0.209\epsilon^{-1}q_1^2r^{-2}$	1.08960×10^{-1}

Table K.3: Symbolic expressions recovered by VaSST ($K = 3$ and $D = 3$) and competing methods for **CL**: $F = 0.08\epsilon^{-1}q_1q_2r^{-2}$ under $\sigma^2 = 0.2^2$. Out-of-sample RMSE is evaluated on a 10% held-out test set, with all coefficients in the symbolic expression reported up to three decimal places across all methods.

Method	Symbolic Expression Learned	RMSE
VaSST	$-0.016 + 0.096\epsilon^{-1}q_1q_2r^{-2}$	2.00629×10^{-1}
BMS	$0.078\epsilon^{-1}q_1q_2r^{-2}$	2.00976×10^{-1}
BSR	$-1.194 + 0.540 \ln\left(\epsilon^{-1}q_1^2r^{-2}\right) - 0.274 \sin\left(\cos\left(\frac{q_2}{q_1}\right)\right)$	2.01511×10^{-1}
QLattice	$0.075\epsilon^{-1}q_1q_2r^{-2} + 0.019$	2.00925×10^{-1}
gplearn	$0.081\epsilon^{-1}q_1q_2r^{-2}$	2.01312×10^{-1}
DEAP	$0.209\epsilon^{-1}q_1^2r^{-2}$	2.04751×10^{-1}

K.1.2 Learning CPE

Table K.4: Symbolic expressions recovered by VaSST ($K = 3$ and $D = 3$) and competing methods for **CPE**: $\Delta U = Gm_1m_2(r_2^{-1} - r_1^{-1})$ under the noiseless setting. Out-of-sample RMSE is evaluated on a 10% held-out test set, with all coefficients in the symbolic expression reported up to three decimal places across all methods.

Method	Symbolic Expression Learned	RMSE
VaSST	$-0.997 Gm_1m_2r_1^{-1} + 1.011 Gm_1m_2r_2^{-1}$	3.66×10^{-3}
BMS	$-Gm_1m_2r_1^{-1} + Gm_1m_2r_2^{-1}$	0.0
BSR	$0.011 + 0.011 \exp\left(\cos\left(\frac{r_2}{r_1}\right)\right) + 0.053 G^2 m_1^4 r_1^{-2}$	8.44849
QLattice	$0.877 \left(Gm_1^2 r_1^{-1}\right) \left(\frac{m_2}{m_1} - 0.018\right) \left(-0.019 \frac{r_2}{r_1} + \exp(-0.161(1 - 0.224 \frac{m_2}{m_1})^2 - 0.243(-0.618 \frac{r_2}{r_1} - 1)^2) + 1.450\right) - 0.002$	3.09445×10^{-2}
gplearn	$-Gm_1m_2r_1^{-1} + Gm_1m_2r_2^{-1}$	8.61×10^{-16}
DEAP	$-Gm_1m_2r_1^{-1} + Gm_1^2r_1^{-1}$	8.32106×10^{-1}

Table K.5: Symbolic expressions recovered by VaSST ($K = 3$ and $D = 3$) and competing methods for **CPE**: $\Delta U = Gm_1m_2(r_2^{-1} - r_1^{-1})$ under noise $\sigma^2 = 0.1^2$. Out-of-sample RMSE is evaluated on a 10% held-out test set, with all coefficients in the symbolic expression reported up to three decimal places across all methods.

Method	Symbolic Expression Learned	RMSE
VaSST	$-0.004 - 0.996 Gm_1m_2r_1^{-1} + 1.017 Gm_1m_2r_2^{-1}$	1.00194×10^{-1}
BMS	$-Gm_1m_2r_1^{-1} + Gm_1m_2r_2^{-1}$	1.00224×10^{-1}
BSR	$0.011 + 0.011 \exp\left(\cos\left(\frac{r_2}{r_1}\right)\right) + 0.053 G^2 m_1^4 r_1^{-2}$	8.44869
QLattice	$-4.351 Gm_1^2 r_1^{-1} \left(1.848(0.116 - 0.121 \frac{m_2}{m_1}) \exp(0.825 \exp(-0.302 \frac{r_2}{r_1})) - 0.279\right) + 0.040$	1.10423×10^{-1}
gplearn	$-Gm_1m_2r_1^{-1} + Gm_1m_2r_2^{-1}$	1.00224×10^{-1}
DEAP	$-Gm_1m_2r_1^{-1} + Gm_1^2 r_1^{-1}$	8.41589×10^{-1}

Table K.6: Symbolic expressions recovered by VaSST ($K = 3$ and $D = 3$) and competing methods for **CPE**: $\Delta U = Gm_1m_2(r_2^{-1} - r_1^{-1})$ under $\sigma^2 = 0.2^2$. Out-of-sample RMSE is evaluated on a 10% held-out test set, with all coefficients in the symbolic expression reported up to three decimal places across all methods.

Method	Symbolic Expression Learned	RMSE
VaSST	$0.002 - 0.997 Gm_1m_2r_1^{-1} + 1.020 Gm_1m_2r_2^{-1}$	2.00318×10^{-1}
BMS	$-Gm_1m_2r_1^{-1} + Gm_1m_2r_2^{-1}$	2.00448×10^{-1}
BSR	$0.011 + 0.011 \exp\left(\cos\left(\frac{r_2}{r_1}\right)\right) + 0.053 G^2 m_1^4 r_1^{-2}$	8.45008
QLattice	$0.199 Gm_1m_2r_1^{-1} \exp\left(0.733 \exp\left(-0.437 \frac{r_2}{r_1}\right)\right) + 0.048$	2.02777×10^{-1}
gplearn	$-Gm_1m_2r_1^{-1} + Gm_1m_2r_2^{-1}$	2.00448×10^{-1}
DEAP	$-Gm_1m_2r_1^{-1} + Gm_1^2 r_1^{-1}$	8.62690×10^{-1}

K.1.3 Learning FCE

Table K.7: Symbolic expressions recovered by VaSST ($K = 3$ and $D = 3$) and competing methods for **FCE**: $F = qE_f + qBv \sin \theta$ under the noiseless setting. Out-of-sample RMSE is evaluated on a 10% held-out test set, with all coefficients in the symbolic expression reported up to three decimal places across all methods.

Method	Symbolic Expression Learned	RMSE
VaSST	$-0.00285 + 0.00318 \sin\left(\frac{2Bv}{E_f}\right) + 0.0012 \theta + 1.068 (q \sin(\theta) Bv + E_f q)$	1.30759×10^{-3}
BMS	$E_f q + qBv \sin(\theta)$	0.0
BSR	0	20.97136
QLattice	$-33.408 + 95.466 \exp\left(-2(0.012 \theta + \exp(-8.892(0.488 - \exp(-0.223(-0.615 \theta - 1)^2)))^2 - 1.530(0.076 E_f q - 1)^2 - 0.915)^2\right)$	14.60774
gplearn	$\left(\frac{\theta}{\theta^2 + E_f q} + 1.143\right) - \left[(E_f q + \frac{\theta}{\theta^2}) \cdot \frac{5.018}{\theta^2 + \theta^2} \cdot (E_f q) + 0.327\right]$	17.82228
DEAP	3.299	20.71117

Table K.8: Symbolic expressions recovered by VaSST ($K = 3$ and $D = 3$) and competing methods for **FCE**: $F = qE_f + qBv \sin(\theta)$ under $\sigma^2 = 0.1^2$. Out-of-sample RMSE is evaluated on a 10% held-out test set, with all coefficients in the symbolic expression reported up to three decimal places across all methods.

Method	Symbolic Expression Learned	RMSE
VaSST	$-0.00286 + 0.00317 \sin\left(\frac{2Bv}{E_f}\right) + 0.0012\theta + 1.068(qBv \sin(\theta) + E_fq)$	1.0031092×10^{-1}
BMS	$E_fq\left(1 + \frac{Bv}{E_f} \sin(\theta)\right)$	1.00532×10^{-1}
BSR	0	20.97185
QLattice	$-417.608\left(-0.005 \frac{Bv}{E_f} + (-0.274\theta - 0.614)(0.329\theta + 0.312) + 0.117\right) \times$ $\exp\left(-1.979(1 - 0.083E_fq)^2 - 0.407(-0.620\theta - 1)^2\right) - 5.228$	14.47309
gplearn	$\frac{\theta}{E_fq} - (E_fq[0.378 + \mathcal{A}] + 0.327),$ $\mathcal{A} = \left(-0.888 + \frac{Bv}{E_f}\right) \frac{E_fq\theta}{\theta^2 + 1} \frac{\mathcal{B}}{\theta^2 + E_fq},$ $\mathcal{B} = \left(-0.888 + \frac{Bv}{E_f}\right) (1.086\theta) \frac{\mathcal{D}}{\theta^2 + E_fq} - 1,$ $\mathcal{D} = \frac{\theta}{E_fq} + 2.431E_fq + \frac{Bv}{E_f} + 4.162 - 3.322 \frac{E_fq}{\theta^2} + 2.163 \frac{E_fq}{\theta^4}.$	18.08813
DEAP	3.299	20.71197

Table K.9: Symbolic expressions recovered by VaSST ($K = 3$ and $D = 3$) and competing methods for **FCE**: $F = qE_f + qBv \sin(\theta)$ under $\sigma^2 = 0.2^2$. Out-of-sample RMSE is evaluated on a 10% held-out test set, with all coefficients in the symbolic expression reported up to three decimal places across all methods.

Method	Symbolic Expression Learned	RMSE
VaSST	$-0.00287 + 0.00316 \sin\left(\frac{2Bv}{E_f}\right) + 0.0012\theta + 1.068(qBv \sin(\theta) + E_fq)$	1.92190×10^{-1}
BMS	$E_fq\left(1 + \frac{Bv}{E_f} \sin(\theta)\right)$	2.01063×10^{-1}
BSR	0	20.97282
QLattice	$151.935 \exp\left(-0.033(0.746\theta - 1)^2 - 2 \exp(-0.251(1 - 0.207\theta)^2\right.$ $\left. \times (-0.054E_fq - 0.764\theta - 1)^2\right) - 34.930$	14.25160
gplearn	$\frac{\theta + E_fq}{\theta\left(0.144 + (\theta + E_fq) \frac{\mathcal{N}}{\mathcal{D}}\right)},$ $\mathcal{D} = -1.143 + 0.823 \frac{E_fq}{\theta^3} \left[\left(\frac{2\theta}{E_fq} - \frac{\theta}{\theta^2 + E_fq} \right) \right.$ $\left. + \left(0.512E_fq + \frac{\theta^2}{\left(\frac{Bv}{E_f}\right)\left(\frac{\theta}{E_fq} + 1.143\right)} + 0.807 \right) \right],$ $\mathcal{N} = \frac{\theta^2}{\frac{Bv}{E_f}} - \left[\left(\frac{\theta}{E_fq} + 0.512E_fq + \frac{\theta^2\left(\frac{Bv}{E_f} + 0.365\right)}{5.018\left(\frac{Bv}{E_f}\right)^2} + 0.807 \right) \frac{\theta}{E_fq} \right].$	18.40486
DEAP	3.299	20.71325

K.1.4 Learning FTC

Table K.10: Symbolic expressions recovered by VaSST ($K = 3$ and $D = 3$) and competing methods for **FTC**: $P = \kappa A(T_2 - T_1)d^{-1}$ under the noiseless setting. Out-of-sample RMSE is evaluated on a 10% held-out test set, with all coefficients in the symbolic expression reported up to three decimal places across all methods.

Method	Symbolic Expression Learned	RMSE
VaSST	$0.001 - 0.975 \frac{\kappa AT_1}{d} + 0.999 \frac{\kappa AT_2}{d}$	1.26016×10^{-2}
BMS	<i>BMS failed to return valid expression</i>	–
BSR	$0.807 - 0.103 \exp\left(\cos\left(\frac{d}{\sqrt{A}}\right)\right) + 0.151 \kappa^2 AT_1^2$	3.93763×10^{-1}
QLattice	$\left(1.000 \frac{T_2}{T_1} - 1.001\right) \frac{\kappa AT_1}{d}$	1.21977×10^{-4}
gplearn	$\frac{\kappa A(T_2 - T_1)}{\kappa \sqrt{A} T_2^5 T_1^{-4}}$	1.73076×10^{-16}
DEAP	$\kappa \sqrt{A} T_1 + 4.828 + \frac{d}{\sqrt{A}} \left(\left(\frac{T_2}{T_1}\right)^2 + \left(\frac{T_2}{T_1}\right)^3 + \left(\frac{T_2}{T_1}\right)^4 \right)$	6.76437×10^{-4}

Table K.11: Symbolic expressions recovered by VaSST ($K = 3$ and $D = 3$) and competing methods for **FTC**: $P = \kappa A(T_2 - T_1)d^{-1}$ under $\sigma^2 = 0.2^2$. Out-of-sample RMSE is evaluated on a 10% held-out test set, with all coefficients in the symbolic expression reported up to three decimal places across all methods.

Method	Symbolic Expression Learned	RMSE
VaSST	$0.024 - 0.980 \frac{\kappa AT_1}{d} + 1.013 \frac{\kappa AT_2}{d}$	2.00103×10^{-1}
BMS	<i>BMS failed to return valid expression</i>	–
BSR	$0.803 - 0.103 \exp\left(\cos\left(\frac{d}{\sqrt{A}}\right)\right) + 0.150 \kappa^2 AT_1^2$	4.42201×10^{-1}
QLattice	$-1.953(0.062 - 0.288 \frac{T_2}{T_1})(1.621 - 0.117 \frac{d}{\sqrt{A}})(0.293 \kappa \sqrt{A} T_1 + 0.106)$ $-1.953 \exp\left(-2.637(0.031 \kappa \sqrt{A} T_1 - 1)^2 - 31.501(0.167 \frac{d}{\sqrt{A}} - 1)^2\right) - 0.233$	1.99987×10^{-1}
gplearn	$\frac{\kappa A(T_2 - T_1)}{d}$	2.00448×10^{-1}
DEAP	$\frac{\kappa \sqrt{A} T_1 \kappa \sqrt{A} T_1 + \frac{d}{\sqrt{A}} + 4.828 \left(3 \left(\frac{T_2}{T_1}\right)^3 + 2 \left(\frac{T_2}{T_1}\right)^2 + \frac{T_2}{T_1} + 1\right)}{\left(\frac{T_2}{T_1}\right)^2 \left(\kappa \sqrt{A} T_1 + \frac{d}{\sqrt{A}} + 4.828 \left(3 \left(\frac{T_2}{T_1}\right)^3 + 2 \left(\frac{T_2}{T_1}\right)^2 + \frac{T_2}{T_1} + 1\right) - 2 \frac{d}{\sqrt{A}}\right)}$	2.00172×10^{-1}

K.2 Out-of-sample RMSE for VaSST and Competing Methods

Table K.12: Out-of-sample RMSEs (computed on the 10% held-out test split) of VaSST and competing methods across noiseless and noise levels $\sigma^2 \in \{0.1^2, 0.2^2\}$ for learning Feynman equations in Section 5.2.

Feynman equation	Method	Noiseless	$\sigma^2 = 0.1^2$	$\sigma = 0.2^2$
CL: $F = 0.08 \frac{q_1 q_2}{\epsilon r^2}$	VaSST	4.67×10^{-5}	1.00314×10^{-1}	2.00629×10^{-1}
	BMS	0.0	1.00488×10^{-1}	2.00976×10^{-1}
	BSR	2.29×10^{-2}	1.02342×10^{-1}	2.01511×10^{-1}
	QLattice	4.27×10^{-6}	1.00534×10^{-1}	2.00925×10^{-1}
	gplearn	5.71×10^{-3}	1.00826×10^{-1}	2.01312×10^{-1}
	DEAP	4.51×10^{-2}	1.08960×10^{-1}	2.04751×10^{-1}
CPE: $\Delta U = Gm_1 m_2 (\frac{1}{r_2} - \frac{1}{r_1})$	VaSST	3.66×10^{-3}	1.00194×10^{-1}	2.00318×10^{-1}
	BMS	0.0	1.00224×10^{-1}	2.00448×10^{-1}
	BSR	8.44849	8.44869	8.45008
	QLattice	3.09445×10^{-2}	1.10423×10^{-1}	2.02777×10^{-1}
	gplearn	8.61×10^{-16}	1.00224×10^{-1}	2.00448×10^{-1}
	DEAP	8.32106×10^{-1}	8.41589×10^{-1}	8.62690×10^{-1}
FCE: $F = q(E_f + vB \sin \theta)$	VaSST	1.30759×10^{-3}	1.0031092×10^{-1}	1.92190×10^{-1}
	BMS	0.0	1.00532×10^{-1}	2.01063×10^{-1}
	BSR	20.97136	20.97185	20.97282
	QLattice	14.60774	14.47309	14.25160
	gplearn	17.82228	18.08813	18.40486
	DEAP	20.71117	20.71197	20.71325
FTC: $P = \frac{\kappa A(T_2 - T_1)}{d}$	VaSST	1.26016×10^{-2}	1.00325×10^{-1}	2.00103×10^{-1}
	BMS	–	–	–
	BSR	3.93763×10^{-1}	4.06545×10^{-1}	4.42201×10^{-1}
	QLattice	1.21977×10^{-4}	1.01498×10^{-1}	1.99987×10^{-1}
	gplearn	1.73076×10^{-16}	1.00224×10^{-1}	2.00448×10^{-1}
	DEAP	6.76437×10^{-4}	1.00126×10^{-1}	2.00172×10^{-1}

K.3 Compute Runtimes for VaSST and Competing Bayesian Methods

Table K.13: Single-run compute runtimes (in seconds) of VaSST and competing Bayesian methods under noiseless and noise levels $\sigma^2 \in \{0.1^2, 0.2^2\}$ for learning the Feynman equations in Section 5.2.

Feynman equation	Method	Noiseless	$\sigma^2 = 0.1^2$	$\sigma^2 = 0.2^2$
CL: $F = 0.08 \frac{q_1 q_2}{\epsilon r^2}$	VaSST	85.19	101.52	75.35
	BMS	107.33	110.02	112.47
	BSR	186.44	188.53	190.01
CPE: $\Delta U = Gm_1 m_2 (\frac{1}{r_2} - \frac{1}{r_1})$	VaSST	103.72	108.66	92.79
	BMS	135.34	129.87	127.84
	BSR	180.93	179.74	188.77
FCE: $F = q(E_f + vB \sin \theta)$	VaSST	98.92	114.19	92.95
	BMS	135.30	137.13	130.74
	BSR	180.93	193.00	186.55
FTC: $P = \frac{\kappa A(T_2 - T_1)}{d}$	VaSST	104.23	121.30	91.32
	BMS	184.58	201.51	156.75
	BSR	185.52	214.95	187.56

K.4 Top Symbolic Expressions Learned by VaSST

K.4.1 Learning CL

Table K.14: Top 5 ranked symbolic expressions recovered by VaSST ($K = 3$ and $D = 3$) for a single run across all noise levels when learning **CL**: $F = 0.08\epsilon^{-1}q_1q_2r^{-2}$. Expressions are ranked by minimum in-sample RMSE among $H = 2000$ sampled hard symbolic trees. Coefficients in the symbolic expression reported up to three decimal places.

Rank	Symbolic Expression
Noiseless	
1	$0.080\epsilon^{-1}q_1q_2r^{-2}$
2	$0.080\epsilon^{-1}q_1q_2r^{-2}$
3	$0.080\epsilon^{-1}q_1q_2r^{-2}$
4	$0.079\epsilon^{-1}q_1q_2r^{-2}$
5	$0.079\epsilon^{-1}q_1q_2r^{-2}$
$\sigma^2 = 0.1^2$	
1	$-0.008 + 0.088\epsilon^{-1}q_1q_2r^{-2} - 0.001\epsilon^{-1}q_1^{-1}q_2^3r^{-2}$
2	$-0.006 + 0.087\epsilon^{-1}q_1q_2r^{-2} - 0.001\epsilon^{-1}q_1^{-1}q_2^3r^{-2}$
3	$-0.009 + 0.088\epsilon^{-1}q_1q_2r^{-2} - 0.001\epsilon^{-1}q_1^{-1}q_2^3r^{-2}$
4	$0.018 + 0.083\epsilon^{-1}q_1q_2r^{-2} - 0.009\frac{q_2}{q_1}$
5	$-0.006 + 0.079\epsilon^{-1}q_1q_2r^{-2} + 0.013\epsilon^{-1}q_1^2r^{-2}$
$\sigma^2 = 0.2^2$	
1	$-0.016 + 0.096\epsilon^{-1}q_1q_2r^{-2} - 0.001\epsilon^{-1}q_1^{-1}q_2^3r^{-2}$
2	$-0.012 + 0.095\epsilon^{-1}q_1q_2r^{-2} - 0.001\epsilon^{-1}q_1^{-1}q_2^3r^{-2}$
3	$-0.041 + 0.191\epsilon^{-1}q_1^2r^{-2} - 0.001\epsilon^{-2}q_2^4r^{-4} + 0.002\epsilon^{-1}q_1^{-2}q_2^4r^{-2}$
4	$-0.024 + 0.170\epsilon^{-1}q_1^2r^{-2} + 0.004\epsilon^{-1}q_1^{-1}q_2^3r^{-2}$
5	$-0.024 + 0.170\epsilon^{-1}q_1^2r^{-2} + 0.004\epsilon^{-1}q_1^{-1}q_2^3r^{-2}$

K.4.2 Learning CPE

Table K.15: Top 5 ranked symbolic expressions recovered by VaSST ($K = 3$ and $D = 3$) for **CPE**: $\Delta U = Gm_1m_2(r_2^{-1} - r_1^{-1})$ across all noise levels. Expressions are ranked by minimum in-sample RMSE among $H = 2000$ sampled hard symbolic trees. Coefficients in the symbolic expression reported up to three decimal places.

Rank	Symbolic Expression
Noiseless	
1	$-0.001 + 0.001 G^2 m_1^3 m_2 r_1^{-2} - 0.997 G m_1 m_2 r_1^{-1} + 1.011 \frac{G m_1 m_2}{r_2}$
2	$-0.021 + 0.003 \frac{r_2}{r_1} + 1.015 \frac{G m_1 m_2}{r_2} - 0.999 G m_1 m_2 r_1^{-1}$
3	$-0.009 - 1.007 G m_1 m_2 r_1^{-1} + 1.007 \frac{G m_1 m_2}{r_2}$
4	$0.791 + 0.118 \left(\frac{m_2}{m_1} \frac{G m_1^2 r_1^{-1} + \frac{m_2}{m_1}}{\frac{r_2}{r_1}} + 1 \right) + 1.125 G^2 m_1^3 m_2 r_1^{-2} + 0.087 \frac{G m_1 m_2 r_1^{-1} (G m_1^2 r_1^{-1} + \frac{m_2}{m_1})}{\frac{r_2}{r_1}}$
5	$1.082 - 0.610 \left(\frac{m_2}{m_1} \frac{r_1}{r_2} + G m_1 m_2 r_1^{-1} \right) \frac{\frac{r_2}{r_1}}{G m_1^2 r_1^{-1} + \frac{r_2}{r_1}} - 1.049 G m_1^2 r_1^{-1} + 1.829 G m_1 m_2 r_1^{-1}$
$\sigma^2 = 0.1^2$	
1	$-0.004 - 0.996 G m_1 m_2 r_1^{-1} + 1.017 \frac{G m_1 m_2}{r_2}$
2	$-0.009 + 1.017 \frac{G m_1 m_2}{r_2} - 0.998 G m_1 m_2 r_1^{-1}$
3	$-0.004 - 1.009 G m_1 m_2 r_1^{-1} + 1.009 \frac{G m_1 m_2}{r_2}$
4	$0.789 + 0.118 \left(\frac{m_2}{m_1} \frac{G m_1^2 r_1^{-1} + \frac{m_2}{m_1}}{\frac{r_2}{r_1}} + 1 \right) + 1.124 G^2 m_1^3 m_2 r_1^{-2} + 0.088 \frac{G m_1 m_2 r_1^{-1} (G m_1^2 r_1^{-1} + \frac{m_2}{m_1})}{\frac{r_2}{r_1}}$
5	$1.087 - 0.612 \left(\frac{m_2}{m_1} \frac{r_1}{r_2} + G m_1 m_2 r_1^{-1} \right) \frac{\frac{r_2}{r_1}}{G m_1^2 r_1^{-1} + \frac{r_2}{r_1}} - 1.057 G m_1^2 r_1^{-1} + 1.832 G m_1 m_2 r_1^{-1}$
$\sigma^2 = 0.2^2$	
1	$0.002 + 1.020 \frac{G m_1 m_2}{r_2} - 0.997 G m_1 m_2 r_1^{-1}$
2	$-0.007 - 0.995 G m_1 m_2 r_1^{-1} + 1.024 \frac{G m_1 m_2}{r_2}$
3	$-1.012 G m_1 m_2 r_1^{-1} + 1.012 \frac{G m_1 m_2}{r_2}$
4	$0.787 + 0.119 \left(\frac{m_2}{m_1} \frac{G m_1^2 r_1^{-1} + \frac{m_2}{m_1}}{\frac{r_2}{r_1}} + 1 \right) + 1.123 G^2 m_1^3 m_2 r_1^{-2} + 0.088 \frac{G m_1 m_2 r_1^{-1} (G m_1^2 r_1^{-1} + \frac{m_2}{m_1})}{\frac{r_2}{r_1}}$
5	$-0.604 - 1.253 G m_1 m_2 r_1^{-1}$

K.4.3 Learning FCE

Table K.16: Top 5 ranked symbolic expressions recovered by VaSST ($K = 3$ and $D = 3$) for **FCE**: $F = qE_f + qBv \sin(\theta)$ across all noise levels. Expressions are ranked by minimum in-sample RMSE among $H = 2000$ sampled hard symbolic trees. Coefficients in the symbolic expression reported up to three decimal places.

Rank	Symbolic Expression
Noiseless	
1	$-0.285 + 0.318 \sin\left(\frac{2Bv}{E_f}\right) + 0.012\theta + 1.068(Bvq \sin\theta + E_fq)$
2	$0.667 + 0.054[\sin(E_fq + \theta) + (E_fq + \theta)Bvq] + 1.071(Bvq + \sin\left(\frac{Bv}{E_f}\right)) \sin\theta + 0.165E_fq \sin\left(\frac{Bv}{E_f}\right)$
3	$-0.729 + 0.053(\theta + E_fq\theta^2) + 0.511\frac{Bv}{E_f} + 0.900E_fq\left(1 + \frac{Bv}{E_f}\right) \sin\theta$
4	$0.959 - 33.164 \sin\theta + 5.351[(E_fq + \frac{Bv}{E_f}) \sin\theta + \sin(\sin\theta)] + 0.895E_fq$
5	$-0.964 + 0.085(3E_fq + \frac{Bv}{E_f}\theta) + 0.344(\sin(E_fq) + 2\frac{Bv}{E_f}) + 1.007Bvq \sin\theta$
$\sigma^2 = 0.1^2$	
1	$-0.286 + 0.317 \sin\left(\frac{2Bv}{E_f}\right) + 0.012\theta + 1.068(Bvq \sin\theta + E_fq)$
2	$0.660 + 0.054[\sin(E_fq + \theta) + (E_fq + \theta)Bvq] + 1.071(Bvq + \sin\left(\frac{Bv}{E_f}\right)) \sin\theta + 0.166E_fq \sin\left(\frac{Bv}{E_f}\right)$
3	$-0.727 + 0.053(\theta + E_fq\theta^2) + 0.510\frac{Bv}{E_f} + 0.900E_fq\left(1 + \frac{Bv}{E_f}\right) \sin\theta$
4	$0.956 - 33.165 \sin\theta + 5.351[(E_fq + \frac{Bv}{E_f}) \sin\theta + \sin(\sin\theta)] + 0.895E_fq$
5	$-0.941 + 0.085(3E_fq + \frac{Bv}{E_f}\theta) + 0.342(\sin(E_fq) + 2\frac{Bv}{E_f}) + 1.008Bvq \sin\theta$
$\sigma^2 = 0.2^2$	
1	$-0.287 + 0.316 \sin\left(\frac{2Bv}{E_f}\right) + 0.012\theta + 1.068(Bvq \sin\theta + E_fq)$
2	$0.653 + 0.054[\sin(E_fq + \theta) + (E_fq + \theta)Bvq] + 1.071(Bvq + \sin\left(\frac{Bv}{E_f}\right)) \sin\theta + 0.167E_fq \sin\left(\frac{Bv}{E_f}\right)$
3	$-0.724 + 0.053(\theta + E_fq\theta^2) + 0.509\frac{Bv}{E_f} + 0.901E_fq\left(1 + \frac{Bv}{E_f}\right) \sin\theta$
4	$0.952 - 33.165 \sin\theta + 5.352[(E_fq + \frac{Bv}{E_f}) \sin\theta + \sin(\sin\theta)] + 0.896E_fq$
5	$-0.918 + 0.085(3E_fq + \frac{Bv}{E_f}\theta) + 0.340(\sin(E_fq) + 2\frac{Bv}{E_f}) + 1.008Bvq \sin\theta$

K.4.4 Learning FTC

Table K.17: Top 5 ranked symbolic expressions recovered by VaSST ($K = 3$ and $D = 3$) for **FTC**: $P = \kappa A(T_2 - T_1)d^{-1}$ across all noise levels. Expressions are ranked by minimum in-sample RMSE among $H = 2000$ sampled hard symbolic trees. Coefficients in the symbolic expression reported up to three decimal places.

Rank	Symbolic Expression
Noiseless	
1	$0.015 + 0.999 \frac{\kappa AT_2}{d} - 0.905 \frac{AT_1 \kappa}{d}$
2	$-0.175 + 0.041 \frac{d}{\sqrt{A}} + 0.126 \kappa \sqrt{A} (T_2 - 2T_1) + 2.045 \frac{\kappa AT_2}{d^2} \sqrt{A}$
3	$0.538 - 0.851 \left(1 - \frac{\kappa AT_2}{d}\right) - 0.051 \left(\kappa \sqrt{A} T_1 - \frac{T_2}{T_1} - 1\right)$
4	$-0.321 + 0.774 \frac{\kappa AT_2}{d} + 0.068 \frac{T_2}{T_1} + 0.003 A^{3/2} \kappa^3 T_1^3 \left(\frac{T_2}{T_1} - \kappa \sqrt{A} T_1\right)$
5	$0.141 - 0.764 \frac{T_1}{T_2} + 0.804 \kappa \sqrt{A} T_1 - 0.867 \kappa \sqrt{A} T_1 \left(1 - \frac{T_2 \sqrt{A}}{T_1 d}\right)$
$\sigma^2 = 0.1^2$	
1	$0.020 + 1.006 \frac{\kappa AT_2}{d} - 0.943 \frac{AT_1 \kappa}{d}$
2	$-0.181 + 0.044 \frac{d}{\sqrt{A}} + 0.129 \kappa \sqrt{A} (T_2 - 2T_1) + 1.982 \frac{\kappa AT_2}{d^2} \sqrt{A}$
3	$-0.349 + 0.778 \frac{\kappa AT_2}{d} + 0.075 \frac{T_2}{T_1} + 0.002 A^{3/2} \kappa^3 T_1^3 \left(\frac{T_2}{T_1} - \kappa \sqrt{A} T_1\right)$
4	$0.433 - 0.819 \left(1 - \frac{\kappa AT_2}{d}\right) + 0.041 \kappa \sqrt{A} T_1 - 0.066 \left(\kappa \sqrt{A} T_1 - \frac{T_2}{T_1} - 1\right)$
5	$-0.371 - 0.789 \frac{\frac{d}{\sqrt{A}} - \kappa \sqrt{A} T_1}{\frac{d}{\sqrt{A}}} \frac{T_2}{T_1} + 0.864 \frac{T_2}{T_1}$
$\sigma^2 = 0.2^2$	
1	$0.024 + 1.013 \frac{\kappa AT_2}{d} - 0.980 \frac{AT_1 \kappa}{d}$
2	$-0.377 + 0.756 \frac{\kappa AT_2}{d} + 0.088 \frac{T_2}{T_1}$
3	$-0.384 + 0.087 \frac{T_2}{T_1} + 0.772 \frac{\kappa AT_2^2}{dT_1} - 0.003 \kappa \sqrt{A} T_1 + 0.003 \frac{T_2 \sqrt{A}}{T_1 d}$
4	$-0.388 - 0.785 \frac{\frac{d}{\sqrt{A}} - \kappa \sqrt{A} T_1}{\frac{d}{\sqrt{A}}} \frac{T_2}{T_1} + 0.866 \frac{T_2}{T_1}$
5	$-0.378 + 0.781 \frac{\kappa AT_2}{d} + 0.082 \frac{T_2}{T_1}$